J. Fluid Mech. (1992), *vol.* 238, *pp.* 187–219
Printed in Great Britain

Interfacial mode interactions in horizontal gas–liquid flows

By L. A. JURMAN†, S. E. DEUTSCH‡ AND M. J. McCREADY‖
Department of Chemical Engineering, University of Notre Dame, Notre Dame, IN 46556 USA

(Received 12 February 1991 and in revised form 18 October 1991)

The behaviour of shear-generated interfacial waves in a cocurrent gas–liquid flow in a small rectangular channel is studied experimentally at conditions close to neutral stability. It is found that the linearly most unstable mode, which typically has a frequency of 8–10 Hz and a wavelength 1–4 cm, grows initially – followed immediately by the first overtone. Measurements of the bicoherence spectrum indicate that the overtone and fundamental are coherent in phase, which suggests that energy is transferred from the fundamental to the linearly stable first overtone. This energy transfer mechanism can stabilize the system, as evidenced by data, which shows that the first mode can saturate with a wave slope small as as 0.005. Theory based on weakly nonlinear mode-interaction equations suggests that this steady state should be stable at conditions close to neutral stability where only overtone modes are present. However, under more severe conditions, where the amplitude of the fundamental mode becomes sufficiently large, a subharmonic mode may be excited. The generation of the subharmonic, when it is linearly stable with respect to the flat film base state, can be interpreted as a linear instability of the steady state containing the fundamental and overtones. Modes that are sidebands (with wavenumbers = $k \pm \delta k$) to the main peak may also occur. These can participate in interactions with low-frequency modes (i.e. δk) and thereby transfer energy to frequencies much below the fundamental. It is expected that all of these interactions play important roles in determining the wave spectrum of conditions far away from neutral stability.

1. Introduction

Stratified gas–liquid flows are found in a wide variety of industrial process situations (e.g. hydrocarbon transportation pipelines, heat exchange devices) as well as in the environment when the wind blows over a water surface. If the degree of gas shear on the liquid is sufficiently large, interfacial waves will be excited by a mechanism which was first analysed by Miles (1957) where energy is transferred from the gas flow when the pressure variation over a wave is shifted from the exact antiphase location where it would be if the flow were inviscid. The pressure variation phase angle is a complex function of the gas velocity profile, wavelength, fluid properties and the level of gas phase turbulence. If, as typically happens, the pressure minimum is shifted to the leeward side of the crest of a downwind-travelling wave, the component of pressure in phase with the wave slope excites a disturbance by reinforcing the motion of fluid

† Current address: Rohm and Haas Co., PO Box 584, Bristol, PA 19007, USA.
‡ Current address: Department of Chemical Engineering, University of Delaware, Newark, DE 19716, USA.
‖ Author to whom correspondence should be addressed.

particles associated with the wave mode. The initially excited waves are periodic, dynamic waves with wavelengths determined by a balance between energy input from the gas flow and viscous dissipation, which varies as $-\nu c^2 k^2$ (where ν is the kinematic viscosity, c is wave speed and k is wavenumber). For the air–water system, this balance produces initial waves with wavelengths of 1–4 cm for both infinitely deep situations (Gastel, Janssen & Komen 1985) and liquids as shallow as 0.5 cm in small enclosed channels (Hanratty 1983). Although a completely general linear stability study which includes the significant effect of turbulence in the gas and is valid for all wavenumbers is lacking, the processes which control linear growth process seem to be well understood as evidenced by the reasonably good agreement between measured onset conditions, wavelengths, speeds and growth rates (e.g. small channels: Cohen & Hanratty, 1965; Craik 1966; Hanratty 1983; Blennerhassett & Smith 1987; deep layers: Miles 1957; Benjamin 1959; Valenzuela 1976; Kawai 1979; Gastel *et al.* 1985).

In contrast, the understanding of nonlinear processes, which typically act to arrest this growth and can cause saturation of amplitudes, is not nearly so advanced. McGoldrick (1965) discovered that waves in the capillary–gravity range undergo three-wave quadratic interactions if the appropriate resonant conditions are met. Subsequent experiments (McGoldrick 1970; Bannerjee & Korpel 1982; Henderson & Hammack 1987) have confirmed predictions of McGoldrick and also Simmons (1969). Kim & Hanratty (1971) derived mode-interaction equations for colinear overtone modes which included non-resonant conditions. Their experiments confirmed the basic predictions of the equations which suggest that, depending upon the liquid depth and the wavelength of the fundamental, a number of (non-resonant) overtone modes can be generated. Another prediction is that energy transfer is oscillatory for non-resonant cases.

One avenue of study of shear-generated wave fields is to develop equations to describe the steady or transient shape of the wave spectrum. Valenzuela & Laing (1972) used a perturbation approach to develop an equation to describe the energy flux in a wind-generated Gaussian wave field. Phillips (1985) employed a wave-action balance equation, which includes energy input, transfer and dissipation (primarily by wave breaking) to describe the equilibrium range of ocean waves. Lleonart & Blackman (1980) combined the idea of a saturated equilibrium range with dimensional arguments to derive an equation to predict the high-frequency portion of the wave spectrum for a cocurrent gas–liquid flow in a small channel. McCready (1986) used a dynamic energy balance, with energy transfer caused by mode-interactions, to develop an expression for the high-frequency part of the spectrum in a gas–liquid flow. However, these last two expressions make no predictions about the amplitude of the largest waves, which for enclosed flows exert the greatest influence on the pressure drop and other properties. Bruno & McCready (1989) provide a partial remedy for this situation by including energy input into the wave spectrum energy balance. Their theory provides a reasonable interpretation of experimental data but requires an arbitrary constant that has to be fit to experimental data.

Interest in the study of the detailed behaviour of shear-generated waves was spurred by experiments by Choi (1977) who observed period doubling, where the dominant frequency changes from about 15 Hz to about 7.5 Hz, for interfacial waves in a cocurrent gas–liquid flow. An explanation for this phenomena was suggested by Chen & Saffman (1979) who determined that a bifurcation in the permanent inviscid wave form can occur if the amplitude becomes sufficiently large; their results are in qualitative agreement with the data of Choi (1977). Bontozoglou & Hanratty (1990)

show that this period-doubling bifurcation depends significantly on the speed of the gas flow and were able to explain Choi's data more closely quantitatively than Chen & Saffman (1979). Bontozoglou & Hanratty (1990) suggest that the observed period doubling is associated with a Kelvin–Helmholtz instability of finite-amplitude waves. A somewhat different approach to this problem has been taken by Janssen (1986). Instead of constructing the Lagrangian for the inviscid equations, he performed a weakly nonlinear, weakly viscous expansion of the entire Navier–Stokes equations. In his formulation, wave growth of the original fundamental is included. The resulting equations describe the evolution of two weakly nonlinear wave modes, the fundamental and the subharmonic. These equations suggest that the period doubling occurs through quadratic interactions between the fundamental and subharmonic (the mechanism is presumably phase-dependent constructive reinforcement of the orbital motions associations with each mode) and provide some insight into the timescale of the period-doubling process. His result, that the fundamental must reach a threshold amplitude before significant energy transfer occurs, agrees with the predicted bifurcation for sufficiently large amplitude found by Chen & Saffman (1979) and Bontozoglou & Hanratty (1990). A second paper, Janssen (1987), uses an energy formulation to derive equations for an arbitrary number of modes; integration of these equations for 50 modes demonstrates the flow of energy in the entire spectrum. Gastel (1987) uses a slightly different formalism to develop equations for the initial development of the three-dimensional spectrum. Recent theoretical work by Cheng & Chang (1990, 1992) suggest that shear-generated waves may be unstable to sideband disturbances and subharmonic mode generation, depending upon the conditions. Their analyses apply to any system for which mode-interaction equations are available (or can be derived). These predictions have not yet been verified experimentally.

In this study, the wave field of a cocurrent gas–liquid flow in a rectangular channel at conditions close to neutral stability is examined. The experiments were done in an attempt to determine the generic behaviour that occurs on sheared liquid layers just above neutral stability. It was found that the liquid depth played a profound role in determining the types of interactions that were seen, while the gas velocity was less important. Consequently, experiments were done at varying liquid flow rates with the gas flow adjusted to a value just sufficient to produce measurable waves. Initially, a two-dimensional fundamental wave, which corresponds closely to the prediction of the fastest growing mode from linear stability, was observed along with one or more (linearly stable) overtones. Measurements of bicoherence spectra demonstrated that the fundamental and overtones have coherent phases and are nonlinearly coupled. Stabilization provided by transfer of energy to overtones, which can dissipate it, causes the fundamental to saturate at a small amplitude-to-wavelength ratio. This suggests that weakly nonlinear theories may provide good predictions of behaviour. The data show that sideband interactions and/or subharmonic generation may also occur at conditions close to neutral stability. To aid in interpretation of these measurements, a set of weakly nonlinear mode-interaction equations that include the effect of gas shear and finite depth are derived.

2. Theory

2.1. *Linear mode evolution*

Experiments presented below will demonstrate that, close to neutral stability, interfacial waves exist as identifiable modes than may saturate with small wave

slopes (amplitude to wavelength ratios) and may interact to form overtones, subharmonics and sidebands. If we first consider the linear stability problem of a gas flowing over a liquid, the flow will be governed by Orr–Sommerfeld equations for the gas and liquid, and boundary conditions which are given (for example) by Valenzuela 1976; Kawai 1979 or Gastel *et al.* 1985. In the present situation, where the flow is confined to a channel, no-slip boundary conditions for the velocities at the wall will be appropriate. For our channel flows, the liquid will be laminar. However, the gas will be turbulent which prevents exact calculation of even the average profile (although it could certainly be predicted with the aid of a turbulence model). In addition, the Orr–Sommerfeld equation for the gas should contain additional terms that represent turbulent contributions to the Reynolds stress as discussed by Thorsness, Morrisroe & Hanratty (1978).

To determine the linear growth/decay behaviour of waves, it is common to assume that all dependent variables are periodic in x, the flow direction, (variation in the transverse direction could be included as well) and may travel and grow or decay with time. This leads to fluctuations associated with a mode of the form

$$\xi(x,t,y) \sim \phi(y)\exp(\mathrm{i}k(x-ct)), \tag{1}$$

where t is time, y is the direction normal to the interface, $\mathrm{i} = \sqrt{-1}$, k is the (real) wavenumber and c is the complex wave speed. If $\mathrm{Im}[c] > 0$, wave modes are predicted to grow exponentially in time. Various forms of the temporal stability problem have been solved analytically for long waves (small k) by Craik (1966) and Blennerhassett (1980), for large k by Cohen & Hanratty (1965), Gastel *et al.* (1985), and Blennerhassett & Smith (1987). Numerical solutions have been obtained by Valenzuela (1976), Kawai (1979) and Blennerhassett (1980).

For the weakly nonlinear problem, which will be considered next, evolution equations for the amplitudes of the wave modes will be derived. Cases considered will be ones when the wave growth rate is sufficiently small that the timescale for variation in the amplitude caused by growth or decay is long compared to a wave period. For conditions where the liquid is initially smooth and waves form with distance (typical of an open flow where there is no feedback of exit conditions back to the inlet), it is possible that both the flow field and the waves are essentially stable in time. Under these conditions, as discussed by Huerre & Monkewitz (1985) or Huerre (1987), the flow is convectively rather than absolutely unstable and it is more appropriate to consider waves which grow spatially. However, because the present study is confined to conditions where the spatial growth rate is small compared to the wavenumber, spatial evolution can be related to temporal evolution using the group velocity (Gaster 1962). Our present interest is to develop equations capable of describing the qualitative behaviour which is observed among weakly nonlinear wave modes. To keep the analysis as clear as possible, only temporal evolution will be considered and flow conditions will be confined to the vicinity of the neutral stability point.

2.2. *Temporal linear stability*

The linear behaviour of this system will be described by temporarily varying modes with the liquid phase described by an Orr–Sommerfeld equation and the effect of the gas phase entering through boundary conditions as was suggested by Cohen & Hanratty (1965) and Craik (1966). The parameters that describe pressure and shear stress variations of the gas on the liquid will be obtained from relations developed for turbulent flows over solid wavy surfaces as suggested by Hanratty (1983). Hanratty's

(1983) results, as well as recent experiments by Prokopiou, McCready & Chang (1992) indicate that this formulation gives reasonably good predictions of linear and weakly nonlinear behaviour for waves close to neutral stability.

The governing equations and boundary conditions for the linear stability problem are listed in the Appendix. Our interest is the region very close to the neutral stability point where the gas-phase stress variation parameters are of order $1/R_L$. The liquid Reynolds number, R_L, is defined as uh/ν_L, where u is the average liquid velocity, h is the average liquid depth and ν_L is the liquid kinematic viscosity. Both R_L and khR_L will be required to be large compared to unity. Under these conditions the wave velocity to leading order in khR_L is shown by Cohen & Hanratty (1965) to be

$$c_R \equiv \mathrm{Re}\,[c[k]] = u_0 - \frac{u_0'}{2k\coth[hk]} + \left[\left(\frac{u_0'}{2k\coth[hk]}\right)^2 + \frac{1}{\coth[hk]}\left(kT + \frac{g}{k}\right)\right]^{\frac{1}{2}}, \quad (2)$$

where u_0 is the interfacial velocity, u_0' is the interfacial liquid velocity gradient, T is the ratio of the coefficient of surface tension to liquid density and g is the acceleration due to gravity. The linear growth rate, $kc_I \equiv k\,\mathrm{Im}\,[c[k]]$, for $|c_I \ll |c_R|$ is given by

$$kc_I = \left(2(c_R - u_0)\coth[hk] + \frac{u_0'}{k}\right)^{-1}\left\{\frac{\hat{p}_I}{\rho_L} + \frac{\hat{\tau}_R}{\rho_L}\left(\coth[hk] + \frac{u_0'}{k(c_R - u_0)}\right) - 4k\nu_L u_0'\right.$$

$$\left. - 4\nu_L k^2(c_R - u_0)\coth[hk] - \frac{k^{\frac{3}{2}}(c_R - u_0)^2(\coth^2[hk] - 1)}{(2hc_R/\nu_L)^{\frac{1}{2}}}\right\}. \quad (3)$$

In (3), ρ_L is liquid density, $\hat{p}_I$ is the component of the interfacial pressure in phase with the wave slope and $\hat{\tau}_R$ is the component of the interfacial shear stress in phase with the wave height. It can be seen that because kh is $O(1)$, khc_I/u_0 will be (and is confined to) $O(R_L^{-1})$.

The waves that occur in small flow systems, particularly when the liquid viscosity is $O(10$ cP), have wavenumbers of $O(1)$ which, for R_L of interest here, is below the accurate range of (3), but still too large for the boundary-layer theory of Jurman & McCready (1989). This limitation could be overcome by a complete numerical solution of the eigenvalue problem for all wavenumbers or, as will be done here, by interpolation of growth rate and speed between the two available theories. Figure 1 shows a typical calculation of wave speed and growth rate close to neutral stability for conditions used in one of the experiments presented below. It is seen that little uncertainty arises when the wave speed is interpolated. The potential error is much larger for the growth rates. However, in the absence of a more elaborate analysis, the interpolated values will be used to interpret the experiments. It is useful to note that wave speed varies only by about 10% between $k = 1$–4 indicating the waves are only slightly dispersive.

2.3. *Weakly nonlinear mode equations*

The existence of experimentally observed steady waves indicates that the rate of energy transfer from unstable to stable modes is balanced by the rate of linear growth. Furthermore, these steady states often occur when the wave slope is in the range of 0.01. Consequently, it should be possible to develop a weakly nonlinear formulation to describe the balance between linear growth/decay processes and nonlinear energy transfer. Several possible ways of ordering of terms in the derivation are possible – but none seem to be wholly satisfactory if a completely analytical formulation is desired. However, if R_L is large enough for viscous effects

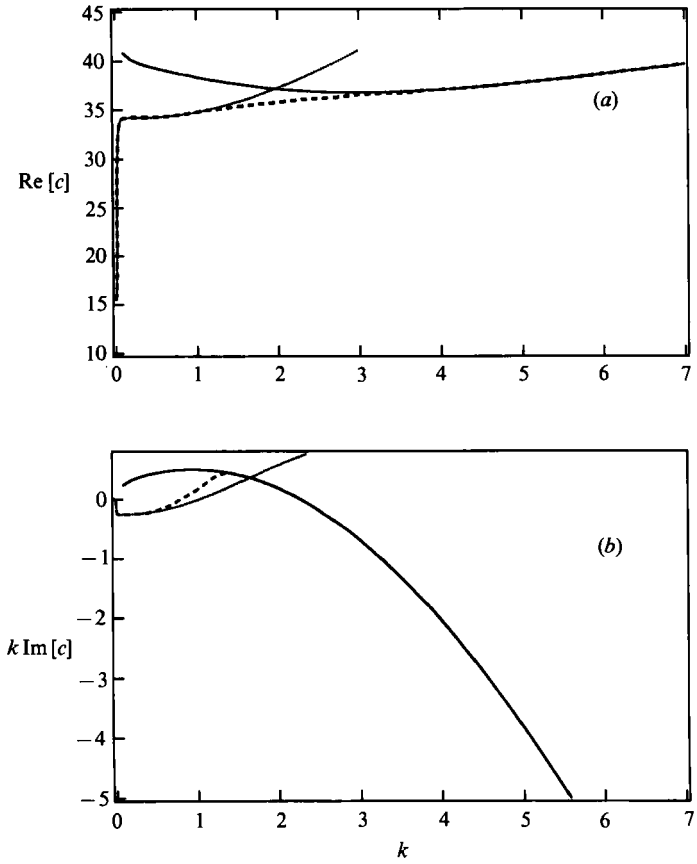

FIGURE 1. Predicted linear stability behaviour for conditions close to neutral stability: $h = 0.651$cm, $v^* = 0.54$ cm/s, $R_L = 70$, $R_G = 4000$, $U_{air} = 3$ m/s, $\mu_L = 9.5$ cP. ——, Deep layer; ....., boundary layer; – – –, interpolated.

to be confined to thin boundary layers near the interface and bottom wall, if the growth rate and wave speed dispersion are $O(1/R_L)$ and if the wave slopes of quadratically interacting waves are $O(u_0/(h\omega R_L))$, where ω is circular frequency, then Janssen's (1986) formulation can be adapted to our system. In our case, the liquid has finite depth and the modes will be assumed not exactly resonant so that a linear dispersion term will arise. It is noted that Kim & Hanratty (1971) have demonstrated significant energy transfer between non-resonant waves. If the flow is inviscid, non-resonant energy transfer will be oscillatory. However, in the presence of viscosity continuous transfer from unstable to stable modes is possible.

An outline, which closely follows Janssen's (1986) analysis of the simplification of the Navier–Stokes equations and boundary conditions into a set of mode-interaction equations is given in the Appendix. For the reasons mentioned above, only temporal evolution is considered and the resulting equations are quite similar to the Fourier-transformed Navier–Stokes equations derived by Qian (1983) for the modal interactions of turbulence. The resulting equations are

$$\dot{A}_l[t] = (\mathrm{i}L_l + lkc_1[lk])\,A_l - \frac{\mathrm{i}\Omega^2 k}{(2l\Omega K_l - u_0')}\left(\sum_{j=l+1}^{n} P_{jl}A_j A_{j-l}^* + \sum_{j=1}^{l-1} Q_{jl}A_{l-j}A_j\right), \qquad (4)$$

where A_l represents the complex wave amplitudes ($a^2 = 4A_l A_l^*$, where a is amplitude), k is the wavenumber of the fundamental, the dot represents a derivative with respect to time, $\Omega \equiv \omega - ku_0$, and n is the total number of included modes. The linear (temporal) growth coefficients, $lkc_{\mathrm{I}}[lk]$, can be obtained from (2) (or a more exact calculation). Additional terms are given by

$$L_l = \frac{(l^2 K_l \Omega^2 + l u_0' \Omega - lgk - l^3 Tk^3)}{(2l\Omega K_l - u_0')}, \tag{5a}$$

$$K_l = \coth[lkh], \tag{5b}$$

$$P_{jl} = l(l(j-l)K_l K_{j-l} + jlK_l K_j + j(j-l)K_j K_{j-l} - (j^2 - l(j-l))), \tag{5c}$$

$$Q_{jl} = \frac{l}{1+\delta[l-2j]}(l(l-j)K_l K_{l-j} + jlK_l K_j + j(l-j)K_j K_{l-j} - (j^2 + l(l-j))), \tag{5d}$$

where $\delta[l-2j] = 1$ if $l-2j = 0$ otherwise $\delta[l-2j] = 0$. The L_l term accounts for the degree of mismatch in the speeds between the fundamental and each of the free modes and is identically 0 for $l = 1$. These equations reduce to those of Kim & Hanratty (1971) if the u_0 and u_0' are zero and to Janssen's (1986) in the limit of small interfacial shear, if the depth is extended to infinity and only two modes considered. It may appear that (4) could be used to obtain an arbitrarily large number of modes, to enable coverage of all possible wavenumbers if the fundamental is taken to be small. However, it must be emphasized that (4) will only be strictly valid if the dispersion and wave damping/growth rates are $O(1/(khR_{\mathrm{L}}))$ and if viscous effects are important in the interaction coefficients.

Experiments at conditions close to neutral stability will demonstrate that typically a fundamental mode, which corresponds to the linearly most unstable mode, will be formed followed immediately by the first overtone, which is linearly stable and can provide stabilization to produce a steady state. If we consider two modes, the fundamental and first overtone, of (4) we get

$$\dot{A}_1 = d_1 A_1 - \mathrm{i}P_1 A_2 A_1^*, \tag{6a}$$

$$\dot{A}_2 = (\mathrm{i}L_2 + d_2)A_2 - \mathrm{i}Q_2 A_1^2, \tag{6b}$$

with

$$P_1 = \frac{\Omega^2 k}{2\Omega K_1 - u_0'} P_{21}, \quad Q_2 = \frac{\Omega^2 k}{4\Omega K_2 - u_0'} Q_{12}, \tag{6c, d}$$

and $d_l = lkc_{\mathrm{I}}[lk]$. This reduction in the number of modes can be justified either by noting that, close to neutral stability, modes higher than the first overtone are damped strongly enough that their wave slopes are very small (the experiments provide confirmation of this) or by doing an extended centre manifold projection (Wiggins 1990; Guckenheimer & Holmes 1983; Cheng & Chang 1990, 1992) of the system, which amounts to expressing all modes higher than the second as nonlinear powers of A_1, A_1^*, A_2^* and A_2. The result of this transformation is (6) plus additional cubic terms. These cubic terms, which are a projection of the quadratic interactions of the fundamental and overtone with higher modes, are then neglected relative to quadratic terms because the magnitudes of A_1, A_1^*, A_2^* and A_2 are found (experimentally) to be small compared with unity.

Perhaps the most important feature of the mode system is apparent in (6). The second mode contains the term $Q_2 A_1^2$. Because of this, energy is fed into the second

mode as soon as the first mode grows to a significant size. Consequently, the second mode will always exist (i.e. be greater than exponentially small) whenever the first mode is unstable. If the growth coefficient for the second mode is negative and sufficiently large in magnitude, then it is possible for the two-mode system to be stable with a net transfer of energy from the first mode to the second mode occurring. To see this, we first write (6) in terms of purely real quantities which gives three equations

$$\dot{b}_1[t] = d_1 b_1[t] + P_1 \sin[\phi[t]]\, b_1[t]\, b_2[t], \tag{7a}$$

$$\dot{b}_2[t] = d_2 b_2[t] - Q_2 \sin[\phi[t]]\, b_1[t]^2, \tag{7b}$$

$$\dot{\phi}[t] = L_2 - Q_2 \frac{\cos[\phi[t]]\, b_1[t]^2}{b_2[t]} + 2P_1 \cos[\phi[t]]\, b_2[t], \tag{7c}$$

where $\phi = \gamma_2 - 2\gamma_1$, $A_1 = \frac{1}{2} b_1 \exp[ikx - \omega t]$, $\gamma_l = \cos^{-1}[2\,\mathrm{Re}[A_l]/b_l]$, and $\mathrm{Re}[A_l] = \frac{1}{2}(A_l + A_l^*)$. It is convenient to simplify these equations further by absorbing the nonlinear coefficients, which do not change the qualitative behaviour of the system, into the amplitudes and by making the variable transformations,

$$a_1 = \frac{-b_1 (P_1 Q_2)^{\frac{1}{2}}}{d_2}, \quad a_2 = \frac{-b_2 P_1}{d_2}, \quad \xi = \frac{-t}{d_2}. \tag{8a–c}$$

This results in the equations

$$\dot{a}_1[\xi] = \Gamma a_1[\xi] + \sin[\phi[\xi]]\, a_1[\xi], a_2[\xi], \tag{9a}$$

$$\dot{a}_2[\xi] = -a_2[\xi] - \sin[\phi[\xi]]\, a_1[\xi]^2, \tag{9b}$$

$$\dot{\phi}[\xi] = \Delta - \frac{\cos[\phi[\xi]]\, a_1[\xi]^2}{a_2[\xi]} + 2\cos[\phi[\xi]]\, a_2[\xi],$$

where $\Gamma = -d_1/d_2$ and $\Delta = -L_2/d_2$. With these definitions, Γ is zero at neutral stability and is positive above neutral stability if $d_1 > 0$ and $d_2 < 0$, which is the only case considered here. The parameter Δ is zero at resonance and can be either positive or negative. It will be seen below that its sign has no effect because Δ appears to the second power in all important results.

Algebraic manipulation of (9) is facilitated by use of a transformation of the kind suggested by Vyshkind & Rabinovich (1976): $X = a_2[\xi]\cos[\phi]$, $Y = a_2[\xi]\sin[\phi]$, and $Z = a_1[\xi]^2$. Doing this, (9) become

$$\begin{pmatrix} \dot{X} \\ \dot{Y} \\ \dot{Z} \end{pmatrix} = \begin{pmatrix} -1 & -\Delta & 0 \\ \Delta & -1 & -1 \\ 0 & 0 & 2\Gamma \end{pmatrix} \begin{pmatrix} X \\ Y \\ Z \end{pmatrix} + \begin{pmatrix} 2XY \\ 2X^2 \\ 2YZ \end{pmatrix}. \tag{10}$$

These equations differ in several important aspects from the superficially similar equations for interactions of modes in a plasma studied by Wersinger, Finn & Ott (1980) and Hughes & Proctor (1990). Consequently, it is worthwhile to examine their behaviour.

Our first interest is the steady state of this system. Letting the derivatives be zero we find a non-trivial steady state at

$$X_0 = \frac{\Delta\Gamma}{1-2\Gamma}, \quad Y_0 = -\Gamma, \quad Z_0 = \Gamma + \frac{\Delta^2\Gamma}{(1-2\Gamma)^2} \tag{11}$$

which gives

$$a_1 = \left(\Gamma + \frac{\Delta^2\Gamma}{(1-2\Gamma)^2}\right)^{\frac{1}{2}}, \quad a_2 = \left(\Gamma^2 + \frac{\Delta^2\Gamma^2}{(1-2\Gamma)^2}\right)^{\frac{1}{2}}, \quad \phi = \sin^{-1}\left\{-\left[1+\left(\frac{\Delta}{1-2\Gamma}\right)^2\right]^{-\frac{1}{2}}\right\}. \tag{12a–c}$$

If the degree of mismatch is small, $a_1 \sim \Gamma^{\frac{1}{2}}$ which means that the unscaled amplitude b_1 varies as $(d_1 d_2/(P_1 Q_2))^{\frac{1}{2}}$ or (roughly) $(d_1 d_2)^{\frac{1}{2}}/(\omega k)$. This indicates that amplitudes are increased by a greater growth rate and diminished by a faster interaction rate (which increases with wavenumber and frequency). Note that the presence of d_2 in the numerator occurs because as d_2 increases, a_2 decreases, which limits the rate at which energy can be removed from the first mode. The effect can be seen by reference to (9*a*, *b*). When $\phi \approx -\frac{1}{2}\pi$, energy transfer is monotonic from the fundamental to the first overtone and, consequently, increases in $a_2[\xi]$ actually act to reduce the magnitude of $a_1[\xi]$. This suggests a nonlinear means for wave damping. To investigate the physical effect of the frequency mismatch parameter, Δ, which controls the efficiency of nonlinear transfer, we expand (12*c*) around $\Delta = 0$,

$$\phi = -\tfrac{1}{2}\pi + \frac{|\Delta|}{1-2\Gamma} - \frac{|\Delta|^3}{3(1-2\Gamma)^3} + \frac{|\Delta|^5}{5(1-2\Gamma)^5} + O(|\Delta|^7), \tag{13a}$$

and also large Δ,

$$\phi = -\frac{1-2\Gamma}{|\Delta|} + \frac{(1-2\Gamma)^3}{3|\Delta|^3} - \frac{(1-2\Gamma)^5}{5|\Delta|^5} - O(|\Delta|^{-7}). \tag{13b}$$

The phase angle is $-\frac{1}{2}\pi$ in the event of no mismatch. When this value of ϕ is placed into (7*a*) and (7*b*), energy transfer from the fundamental to the first overtone is maximized because $\sin(-\frac{1}{2}\pi) = -1$. When Δ is large, $\phi \approx 0$ and the efficiency of energy transfer from the fundamental to the overtone is greatly reduced. We see from (12*a*) and (12*b*), as Δ increases from 0, the amplitudes of both modes are increased – consistent with the idea that because energy transfer is no longer as efficient, larger amplitudes are required to stabilize the system. It is interesting to note that the ratio of the amplitudes, which is given by $a_2/a_1 = \Gamma^{\frac{1}{2}}$ does not depend on Δ.

To check the stability of the steady state to infinitesimal perturbations in amplitude or phase (which would be expected to be present in a real flow), (10) are relinearized about $X_0+\delta x$, $Y_0+\delta y$, $Z_0+\delta z$, giving the matrix that governs stability:

$$\begin{pmatrix} -1+2\Gamma & \dfrac{\Delta}{-1+2\Gamma} & 0 \\ -\dfrac{\Delta(1+2\Gamma)}{-1+2\Gamma} & -1 & -1 \\ 0 & \dfrac{2\Gamma(1+\Delta^2-4\Gamma+4\Gamma^2)}{(-1+2\Gamma)^2} & 0 \end{pmatrix}. \tag{14}$$

The three eigenvalues of (14) govern the stability of the steady state. Two of the eigenvalues are complex conjugates with real parts that are always negative and consequently do not contribute to instability. The third, which is always real, is plotted as a function of Γ for various Δ in figure 2. It is seen that the steady state (12) is stable provided that $\Gamma < 0.5$. If $\Gamma > 0.5$, then the steady state is unstable and it is expected that the amplitudes become unbounded. Numerical integrations of (4)

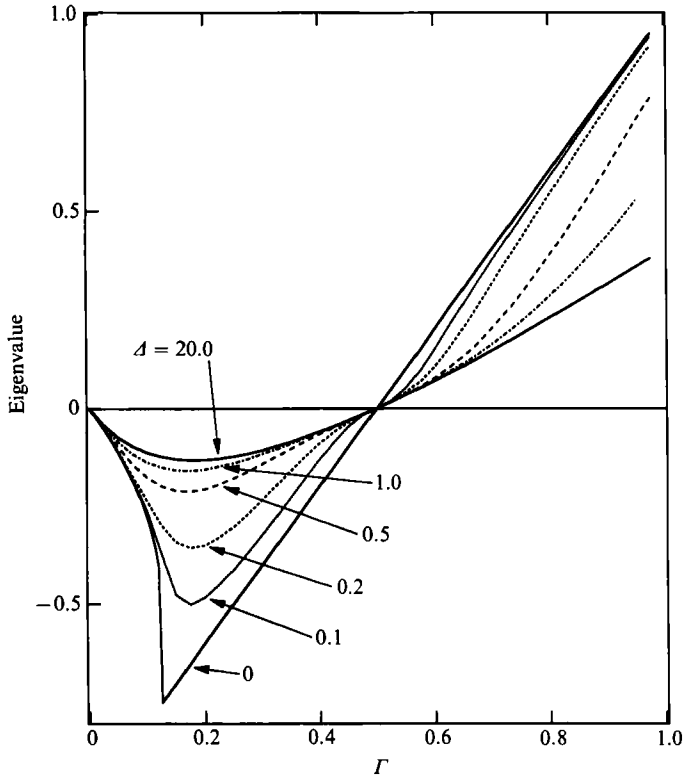

FIGURE 2. Eigenvalue governing stability of (14) for different values of frequency mismatch parameter, Δ.

exhibit this behaviour if only two modes are used. (However, if additional overtone modes are added, the system can still be stabilized.) The frequency mismatch parameter, Δ, does not change the system from stable to unstable but it does affect the rate at which it may approach stability through the magnitude of the eigenvalues in figure 2. It can be seen from the centre manifold reduction of (10),

$$\dot{Z} = 2\Gamma Z - \frac{2Z^2}{1+\Delta^2} + \frac{(-4+12\Delta^2)Z^3}{(1+\Delta^2)^3} + O(Z^4), \tag{15}$$

that the system bifurcates transcritically as Γ crosses 0. A transcritical bifurcation is consistent with the steady-state stability observed by the values of the eigenvalues. Consequently, in our system we expect that sufficiently close to neutral stability (i.e. $\Gamma < \frac{1}{2}$), the system will evolve into a stable steady state which consists of a fundamental and first overtone. Higher overtones will remain quite small. For more severe cases, when Γ is greater than $\frac{1}{2}$, the amplitudes of the fundamental and first overtone will grow and more (linearly stable) overtones will be magnified to finite values capable of dissipating a sufficient amount of energy. However, the system is expected to remain stable by the same energy transfer mechanism until an instability which involves modes other than overtones (e.g. sidebands or subharmonics) becomes important.

Even though the equations studied by Wersinger *et al.* (1980) or Hughes & Proctor (1990) appear similar to (6), very different behaviour is observed. Their equations

arise from a system essentially like (6) but with $d_2 > 0$ and $d_1 < 0$ so that the overtone is excited and transfer to the subharmonic provides the *only* means of stabilization. In their case, the roles of the nonlinear terms are reversed and the mismatch parameter plays an essential role in determining the stability of the finite-amplitude steady state. For their system, the steady state loses stability through a Hopf bifurcation and various types (e.g. single and multiple period oscillations and chaos) of bounded time-varying behaviour are observed as Γ is varied. This contrasts with the present case, where the behaviour of the steady state, (11), is given by an equation of the form (again by use of centre manifold reduction)

$$\dot{\zeta} \sim (-1+2\Gamma)\zeta + \mathrm{i}\Lambda\zeta^3, \tag{16}$$

where Λ is real and ζ is Z scaled by the matrix of eigenvectors of (14). Consequently, stability is lost as Γ increases across 0.5 by a simple bifurcation and the nonlinear term provides no stabilization. Therefore, if $\Gamma > 0.5$, the amplitudes always diverge to infinity. As mentioned above, for the complete system (4), as Γ increases to 0.5, additional overtone modes that act to stabilize the system will be generated. Consequently, (16) exceeds the limit of realistic physical application of the two-mode model, (6), but provides a basis for comparison with the results of Wersinger *et al.* (1980) or Hughes & Proctor (1990).

2.4. *Subharmonic instability*

Data shown below show a subharmonic peak for certain experimental situations. It is of interest to examine the question of subharmonic stability as predicted by (4). Cheng & Chang (1992) demonstrate that subharmonic instability is governed by the linear instability of the subharmonic mode with respect to the steady state which occurs between the fundamental and its overtones. In terms of the notation used in (6), to leading order in wave slope, the matrix that determines linear stability of the subharmonic becomes

$$\begin{pmatrix} d_{\frac{1}{2}}+\mathrm{i}L_{\frac{1}{2}} & P_{\frac{1}{2}}A_1 \\ P_{\frac{1}{2}}A_1^* & d_{\frac{1}{2}}-\mathrm{i}L_{\frac{1}{2}} \end{pmatrix}, \tag{17}$$

where the subscript $\frac{1}{2}$ denotes the first subharmonic. For the system to be stable, the trace of (17) must be negative, which is the same as requiring the growth rate of the subharmonic to be negative. Even if the growth rate is negative, the subharmonic is still predicted to grow if the real part of one of the eigenvalues of (17) becomes positive. This condition occurs if

$$(d_{\frac{1}{2}})^2 < (P_{\frac{1}{2}})^2 A_1 A_1^* - (L_{\frac{1}{2}})^2, \tag{18}$$

which simply says that the subharmonic mode is predicted to grow if energy fed from the fundamental exceeds the rate at which it can be linearly dissipated. Equation (18) demonstrates that the amplitude of the fundamental plays an important role in this instability. If $A_1 A_1^*$ becomes large enough, the subharmonic will almost certainly form because $d_{\frac{1}{2}}$ and $L_{\frac{1}{2}}$ are generally no larger than $O(1)$ and $P_{\frac{1}{2}} = O(10)$. It is also worth pointing out that the magnitude of mismatch $L_{\frac{1}{2}}$ affects the conditions of instability, which does not happen for either the onset of waves (first positive eigenvalues of (10)) or the point at which the two-mode steady state becomes unstable (as given by the eigenvalues in figure 2). For the present work, the prediction of (18) can be tested by using calculated coefficients along with measured amplitudes of the fundamental.

2.5. *Sideband formation*

Another instability which may be present in linearly unstable dissipative systems and is observed in the data presented here is the 'sideband' instability which has been studied by numerous investigators including Eckhaus (1965), Benjamin & Feir (1967), Lange & Newell (1974), Lin (1974) and Stuart & DiPrima (1978). Sidebands are observed to be peaks located at $\pm\delta k$ (where δ is small) from the main peak at k. A recent paper by Cheng & Chang (1990) (their equation (52)) provides a criterion which, if applied to (4), gives

$$\left(\frac{\partial c_{\mathrm{I}}[k]}{\partial k}\bigg|_{k_0}\right)^2\left(1+\left(\frac{2L_2}{2c_{\mathrm{I}}[k]-c_{\mathrm{I}}[2k]}\right)^2\right) - c_{\mathrm{I}}[k]\left[\left(\frac{-\partial^2 c_{\mathrm{I}}[k]}{\partial k^2}\bigg|_{k_0}\right)+\left(\frac{2L_2}{2c_{\mathrm{I}}[k]-c_{\mathrm{I}}[2k]}\right)\left(\frac{-\partial^2 L[k]}{\partial k^2}\bigg|_{k_0}\right)\right] < 0, \quad (19)$$

where $c_{\mathrm{I}}[k]$ and $L[k]$ are continuous and k_0 refers to the wavenumber at the peak of the growth curve. Note that the effects of low-wavenumber modes (e.g. δk, $2\delta k$) which may participate in the interactions are not included in (19) because (4) are not expected to be valid for such small k. In (19), the first term can cause instability if the fundamental wavenumber does not lie exactly at the peak in the growth curve. This instability can be enhanced by speed dispersion through L_2. Stabilization is provided by the second term of (19) which contains the curvature of the growth curve.

3. Experiments

3.1. *Flow system*

The experiments presented here were done in a horizontal, rectangular flow channel with dimensions 30 cm wide, 2.54 cm high and 9 m long. (The flow system is described more completely by Bruno & McCready 1988, 1989; Bruno 1988 and Jurman 1990). Glycerin–water solutions in the viscosity range 8–20 cP were used as the liquid. The high aspect ratio of the channel eliminates secondary flow patterns and minimizes sidewall effects on the wave field. The rectangular geometry provides (as far as possible) uniform film and wave properties which aid comparison with theoretical results.

3.2. *Wave measurements*

Instantaneous film height is measured using parallel wire conductance probes. Their construction is discussed in detail by Miya, Woodmansee & Hanratty (1971); McCready (1986) and Bruno (1988). Each probe consists of two parallel 0.13 mm diameter wires spaced 2 mm apart which extend vertically through the channel, perpendicular to the direction of flow. An input AC voltage is supplied to one of the two wires in the form of a 30 kHz sine wave with a voltage of about 0.2 V. The signal is conducted through the liquid to the second wire, where a custom-design amplifier/converter circuit measures the conducting current (which is directly proportional to liquid layer thickness) and transforms it into a continuous analog output which is suitable for sampling by a microcomputer. A complete diagram of this circuit, which worked significantly better than previous designs, is given in Jurman (1990). The analog to digital conversion rate is 200 samples/s which is appropriate for the conditions studied here where no significant wave frequencies greater than about 50 Hz were observed.

Wave speeds were measured using two parallel wire conductance probes, displaced by a small distance in the flow direction. The frequency resolution of the probe is determined by the separation distance. Larger separation distances are required to detect and track the longest-wavelength disturbances, while the highest frequency is effectively determined by the wave whose length equals the separation distance. Therefore, a larger separation distance, r, for the probe increases its ability to resolve the lower-frequency modes, but decreases its upper frequency limit. The probes used in this study enable resolution of wave speeds in the approximate effective range of 3–20 Hz for $r = 1.55$ cm, and 5–50 Hz for $r = 0.55$ cm.

4. Data-analysis techniques

4.1. *Spectral analyses*

The frequency distribution, speeds and phase coherence of experimentally observed waves are determined by calculating the power, cross-, and bicoherence spectra, from the Fourier transform of the measured surface height time series. Fourier analysis assumes that the surface height time signal, $x[t]$, can be functionally represented by

$$x[t] = \sum_{j=1}^{N} (X_j \exp[\mathrm{i}\theta jt] + X_j^* \exp[-\mathrm{i}\theta jt]), \tag{20}$$

where the Fourier coefficients X_j are obtained from N measured values of discretely sampled data points, x_l, at time t_l, $l = 1, 2, \ldots, N$. For real valued functions, $X_{-j} = X_j^*$, where * denotes the complex conjugate. These coefficients are used to calculate power, cross- and bicoherence spectra.

The basic assumption in Fourier and spectral analyses is that the measured fluctuating time (or other independent variable) series represents a stationary, ergodic process. This is violated if strong nonlinearities are present in the system; anomalous frequency components result which prevent physical interpretation and analysis of the data. However, because this study focuses on the weakly nonlinear behaviour of waves, the use of spectral analysis to determine the properties of measured two-dimensional wave fields should be valid.

4.2. *Power spectrum*

The spectral power density function of the surface height time series measured over a finite time is calculated from the fourier coefficients $X_j(t)$ by

$$\phi[f_j] = E[X(f_j) X^*(f_j)], \quad j = 0, 1, \ldots, \tfrac{1}{2}N, \tag{21}$$

where f is the frequency in Hz, E is the expected value operator, and N corresponds to the sample size of the measured signal. By definition, the spectral density function, $\phi[f]$, is a real quantity, and consequently phase information contained in the original signal $x[t]$ is lost in the calculation. Physically, $\phi[f]$, may be interpreted as the frequency distribution of the variance of the signal $x[t]$. The average amplitude of the measured waves is then related to $\phi[f]$ by

$$\bar{a}^2 = \int_0^\infty \phi[f]\,\mathrm{d}f. \tag{22}$$

where the above is replaced by a summation for a discrete estimate of the power spectrum.

Methods for calculating the discrete power spectrum from a finite digital signal are described in Bendat & Piersol (1986) and Press *et al.* (1986). Increments of 1024 points, a Hanning window, and the routine 'spectrum' given by Press *et al.* (1986) are used to calculate power spectra; overlapping of windows is used for increased accuracy.

4.3. *Cross-spectrum and cross-coherence*

The cross-spectrum is calculated from two film height signals, $x[t]$ and $y[t]$, recorded by probes positioned in series in the flow direction. Denoting the Fourier coefficients of these signals as $X[f_j]$ and $Y[f_j]$, respectively, the cross-spectral density is given by

$$\phi_{xy}[f_j] = E[X^*[f_j]\,Y[f_j]], \quad j = 0, 1, \ldots, \tfrac{1}{2}N. \tag{23}$$

The cross-spectral density function, $\phi_{xy}[f_j]$, is a complex number which can be written in polar notation as

$$\phi_{xy}[f_j] = |\phi_{xy}[f_j]|\exp[-\mathrm{i}\theta_{xy}[f_j]], \quad \theta_{xy}[f_j] = \tan^{-1}\left[\frac{Q_{xy}[f_j]}{C_{xy}[f_j]}\right], \tag{24a,b}$$

where $Q_{xy}[f_j]$ and $C_{xy}[f_j]$ denote the real and imaginary components of $\phi_{xy}[f_j]$, and θ_{xy} measures the phase shift between $x[t]$ and $y[t]$ at frequency f_j. The time delay, τ_{d}, can then be calculated at frequency f_j from

$$\tau_{\mathrm{d}}[f_j] = \frac{\theta_{xy}[f_j]}{2\pi f_j}, \tag{25}$$

and the corresponding wave speed (units of length per time) is calculated by dividing r, the distance between probes, by τ_{d}.

The correlation between the signals $x[t]$ and $y[t]$ is given by the cross-coherence coefficient, γ^2_{xy}, where

$$\gamma^2_{xy} = \frac{|\phi_{xy}(f_k)|^2}{\phi_{xx}(f_k)\,\phi_{yy}(f_k)} \leqslant 1. \tag{26}$$

The cross-coherence coefficient, γ^2_{xy} may assume values between zero and unity; a value of zero indicates that the two signals are statistically independent, while γ^2_{xy} equal to one denotes complete coherency. A relatively high correlation between signals (i.e. greater than about 0.85) is required for accurate measurements of the time delay between probes.

Power spectral programs were modified to accommodate two time series and to estimate the discrete cross-spectrum as prescribed by Bendat & Piersol (1986). Data are segmented and windowed prior to analysis. Values of the cross-coherence are calculated and found to be sufficiently large ($\gamma^2_{xy} > 0.9$) over a frequency range coincident with significant values of the power spectrum.

4.4. *Bispectrum and bicoherence*

The bispectrum determines phase coherence among wave modes measured by the surface height time series, $x[t]$. It is essentially a triple correlation function in the frequency domain that tests for phase correlation between spectral components satisfying the selection rule $f_3 = f_1 + f_2$. This third-order spectrum is defined by

$$\phi_{xxx}[f_j, f_l] = E[X[f_j]\,X[f_l]\,X^*[f_{j+l}]], \quad j, l = 0, 1, \ldots, \tfrac{1}{2}N. \tag{27}$$

Nonlinear interactions between waves generate spectral components which are necessarily phase coherent, while independently excited modes are characterized by

random phases. The statistical averaging denoted by the expectation operator in (27) results in a non-zero value only if the total phase of the three waves is correlated, i.e. if the waves are nonlinearly coupled. If the waves result from independently excited modes, the individual and sum phase of the components will be random, yielding a zero value for $\phi_{xxx}[f_j, f_l]$. Both sum and difference interactions are accounted for in (27).

The bicoherence spectrum, a bispectrum normalized to eliminate dependence on component amplitudes, is used to determine the extent of coupling between waves and is given by Kim & Powers (1979) as

$$b^2[f_j, f_l] = \frac{|\phi_{xxx}[f_j, f_l]|^2}{E[|X_j X_l|^2]\, E[|X_{j+l}|^2]}, \tag{28a}$$

and

$$\beta[f_j, f_l] = \tan^{-1}\left[\frac{\mathrm{Im}\,[b[f_j, f_l]]}{\mathrm{Re}\,[b[f_j, f_l]]}\right], \tag{28b}$$

where $b^2[f_j, f_l]$ is the bicoherence, and $\beta[f_j, f_l]$ is the biphase, which measures the relative phase between components. Equation (28*a*) is bounded between zero and unity; it takes on a value close to one when a wave at $f_j + f_l$ is phase coherent with waves at f_j and f_l. A zero value results from an absence of coherence, or nonlinear interactions, among components. Because a finite-length time series is used to estimate the bispectrum, a non-zero value will result for even the most random processes. The minimum significant value of bicoherence required for 95% confidence is given by Elgar & Guza (1985) as

$$b^2_{95\%} \geqslant 6/M, \tag{29}$$

where M equals the number of windows used in the calculation. By definition, bispectral methods are capable of analysing data only for weak, quadratic nonlinear interactions. If the system being considered contains higher-order nonlinearities, then higher-order spectra must be invoked. The discrete bicoherence spectrum is estimated using the computational procedures prescribed by Kim & Powers (1979). Two-hundred and fifty overlapped windows of 256 points were found to provide adequate resolution, while maintaining statistical stability.

5. Experimental results

The surface tracing and power spectrum for a 9.5 cP liquid at $R_L = 70$ and $R_G = 4000$, (R_G, the gas Reynolds number, is chosen just large enough for waves to be observed and measured) are shown in figure 3. The measurements were taken at a point 5.6 m from the inlet which is a distance sufficient for the spectrum to have reached a steady state. The tracing exhibits a clear dominant frequency (of $\sim$ 8 Hz) even though there is some irregularity to the waves. It is worthwhile to note the slight 'beating', indicative of either a second mode close to the frequency of the first or the presence of a low-frequency mode. Careful examination of the dominant wave shape reveals a slight asymmetry which is a result of the presence of an overtone mode that generally occurs with a fixed phase relative to the fundamental. The power spectrum of the tracing depicts a sharp fundamental at 8 Hz with some energy in the shoulders, a broad overtone at 14–17 Hz and some evidence of a small peak at less than 1 Hz. From the surface tracing, the amplitude, a, of the dominant waves is seen to be about 0.02 cm; integration of the power spectrum between 7.0 and 8.5 Hz (which is the sharp part of the peak) provides an estimate of the 0.023 cm for

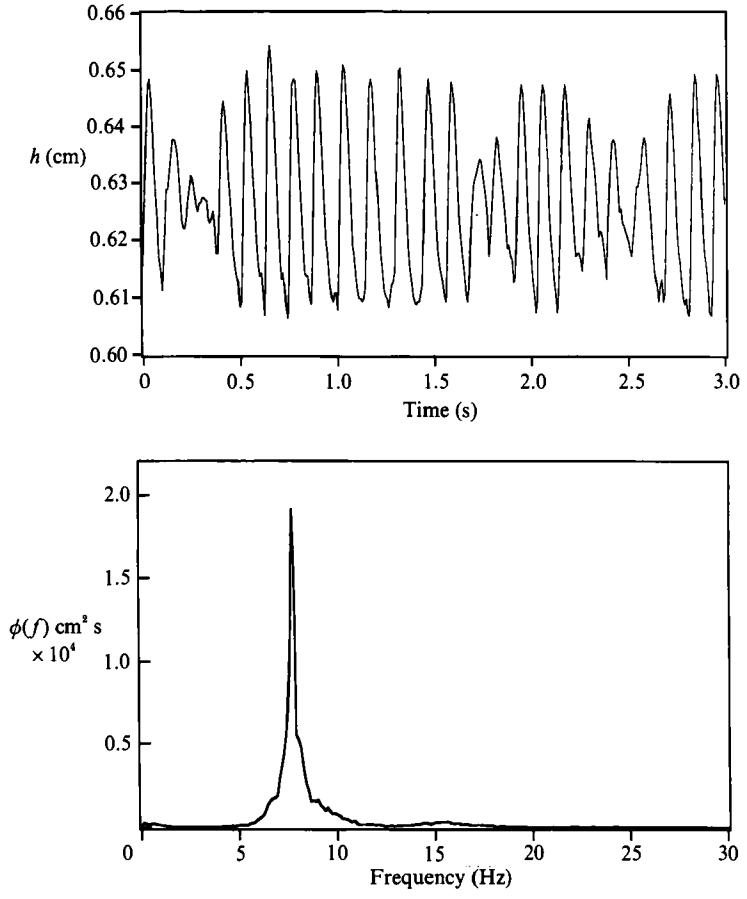

FIGURE 3. Interface tracing at fetch = 5.59 m and power spectrum of waves close to neutral stability: $R_L = 70$, $R_G = 4000$, $U_{air} = 2.9$, $h = 0.65$ cm $\mu_L = 9.5$ cP.

the amplitude. This compares to a wavelength of about 4.1 cm (obtained from measurements of the wave speed); this gives $a/\lambda \approx 0.005$. It is also interesting to view the spectrum plotted as log $[\phi[f]]$ *vs.* f in figure 4. It is clear that there is a slight excess of energy at a frequency which corresponds to the second overtone and a very small, but sharp, peak at the first subharmonic of the fundamental. The role that nonlinear interactions play in distributing energy in the wave spectrum is elucidated by the bicoherence spectrum which is shown as a contour plot in figure 5. The strongest coherence is seen to occur between the fundamental and the first overtone by the selection rule f_1 ($= \sim 8$ Hz) $+ f_1 = f_2$ ($= 16$ Hz) where the peak in coherence is about 0.8 (maximum is 1.0). The phase angle measured between the fundamental and first overtone is $\sim -\frac{1}{4}\pi$. Figure 5 shows that much weaker coherence occurs between f_1, f_2 and f_3($= 24$ Hz), f_2, f_2 and f_4($= 32$ Hz) and also between the low-frequency peak and shoulders of the fundamental. The linear stability curve, shown in figure 1 (*b*), indicates that frequencies near the fundamental are unstable but that the first overtone should be linearly stable. It seems clear that energy from the gas flow fed into the fundamental is transferred to the second mode by nonlinear interaction between the fundamental and the first overtone. This mechanism provides the primary mechanism of stabilization of the spectrum.

Figure 6, which shows the evolution of the spectrum and surface tracing with

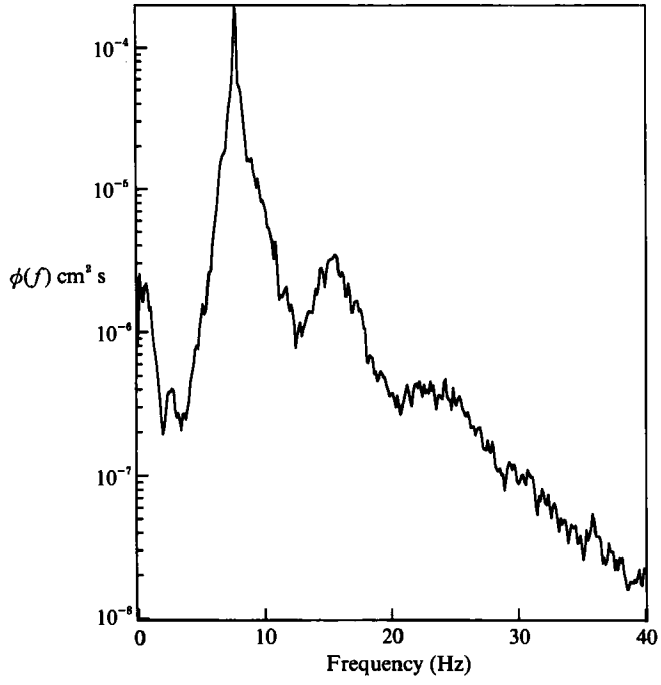

FIGURE 4. Wave spectrum from figure 3 viewed with a logarithmic coordinate.

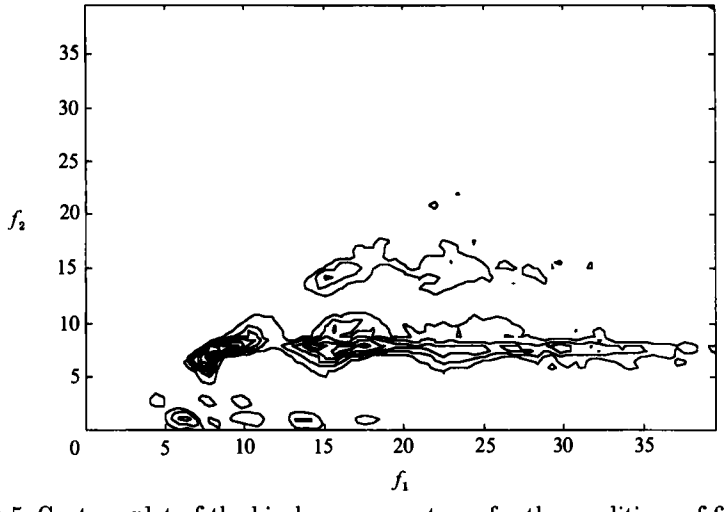

FIGURE 5. Contour plot of the bicoherence spectrum for the conditions of figure 3. Strong coherence between the fundamental and first overtone is shown.

distance for R_L approximately half the value of figure 3, demonstrates growth and stabilization of the fundamental by the appearance of a small-amplitude overtone. The tracings reveal that the phase angle between the fundamental and overtone has shifted from the value in figure 3 (note the rounded crests and sharp troughs) and is now approximately $-\pi$. The bicoherence spectrum initially displays coherence between the fundamental and first overtone. However, as distance in the downstream direction is increased, a strong coherence develops between the fundamental and the first three overtones.

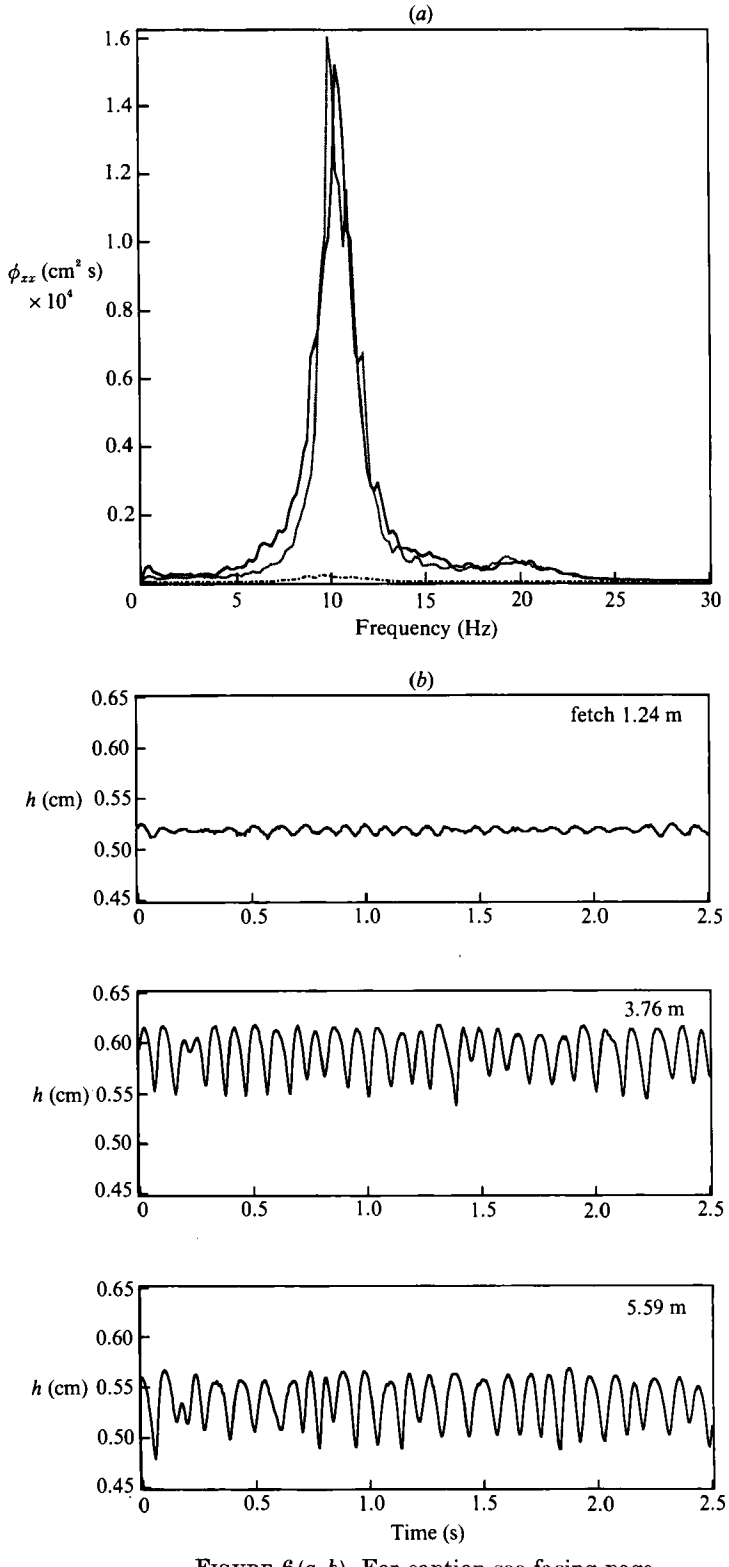

FIGURE 6(*a*, *b*). For caption see facing page.

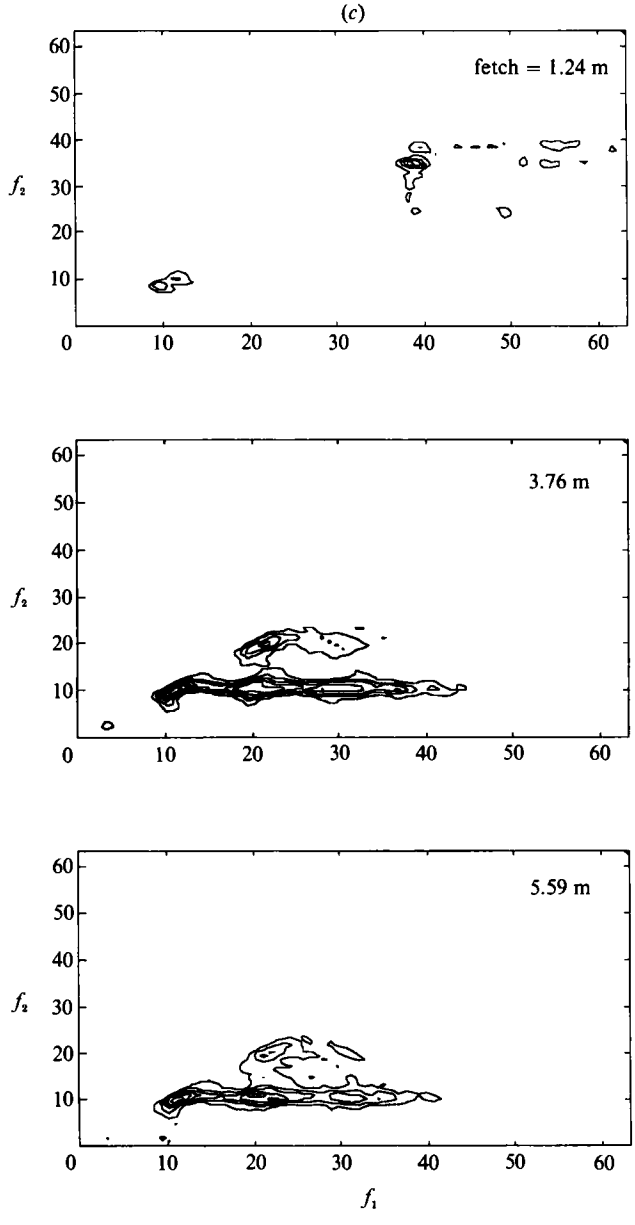

FIGURE 6. (*a*) Wave spectra at increasing fetch for conditions close to neutral stability. (*b*) Surface tracings as a function of fetch. (*c*) Bicoherence of wave field close to neutral stability (contour lines represent $b^2 = 0.1$). $R_L = 35$, $R_G = 4200$, $h = 0.55$ cm, $U_{air} = 3.2$ m/s, $\mu_L = 10$ cP.

If R_L is decreased still further, we see a rather significant qualitative difference in wave evolution as reflected by the spectra of figure 7. A fundamental peak develops and grows significantly between the first and second probes. As distance increases, a subharmonic mode appears and, by the last probe this mode is of comparable size to the fundamental. It is interesting that the subharmonic formation observed on the present finite-depth layer ($h = 0.46$ cm, fundamental wavelength ≈ 2.3 cm) is qualitatively similar to the measurements obtained by Choi (1977) on a layer of

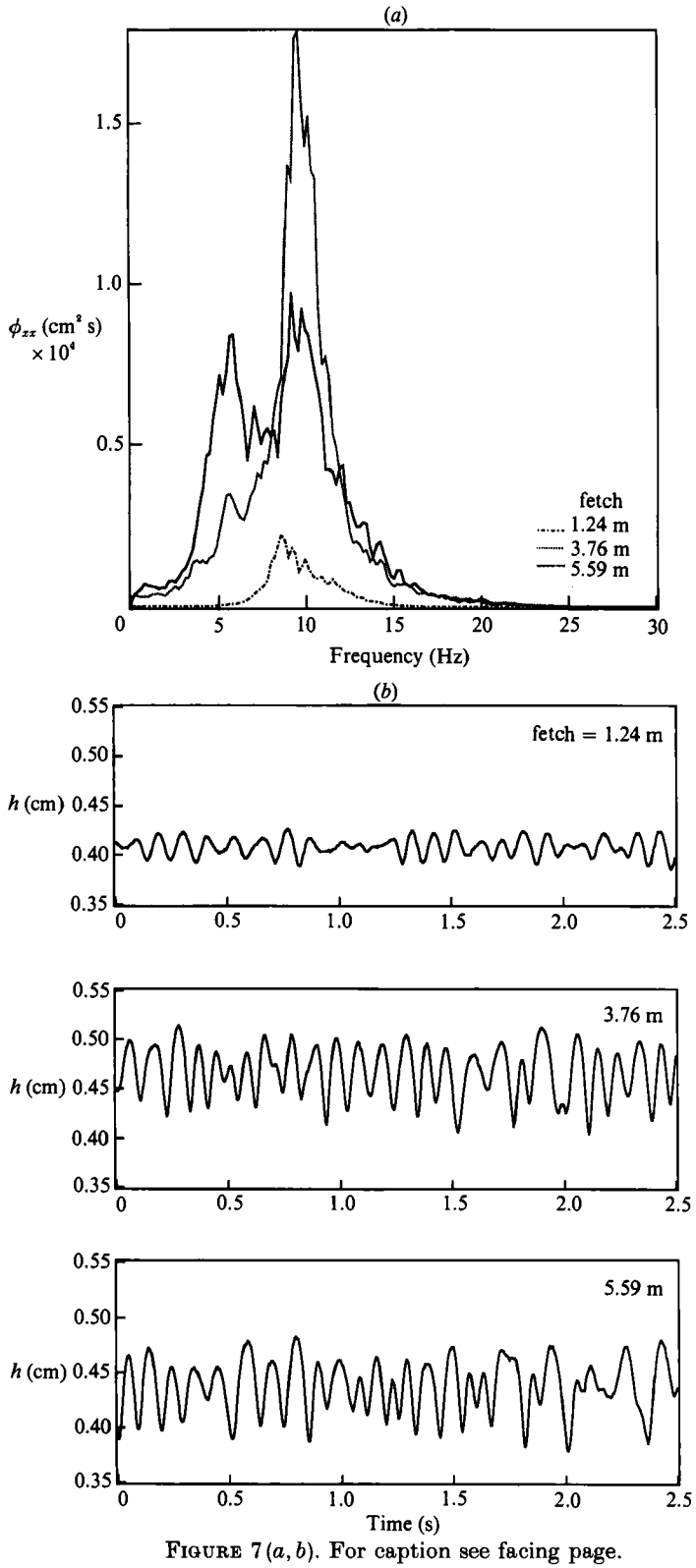

FIGURE 7 (a, b). For caption see facing page.

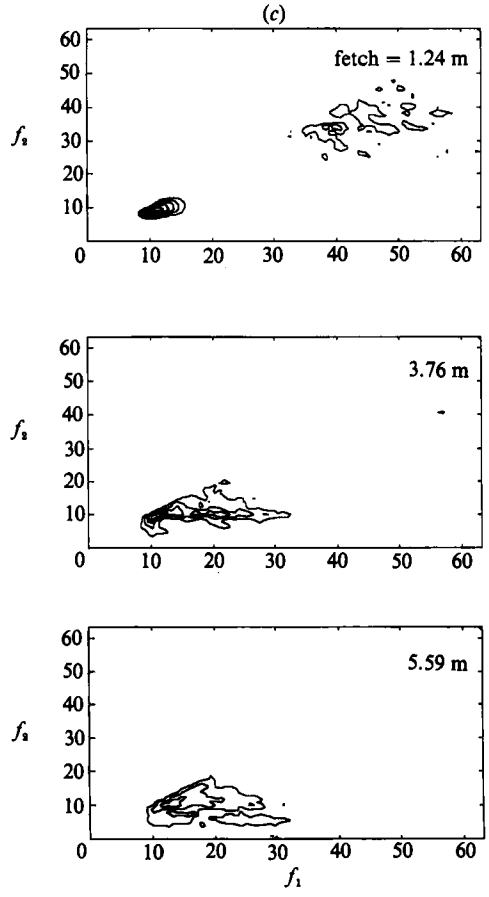

FIGURE 7. (*a*) Wave spectra at increasing fetch for conditions close to neutral stability. A subharmonic appears by the last probe. (*b*) Surface tracings as a function of fetch. (*c*) Bicoherence of wave field close to neutral stability (contour lines represent $b^2 = 0.1$). $R_L = 14$, $R_G = 5150$, $h = 0.45$ cm, $U_{air} = 3.7$ m/s, $\mu_L = 10$ cP.

effectively infinite depth ($h = 26$ cm, fundamental wavelength ≈ 2.4 cm) so that, as will be discussed below, liquid depth is not the only factor determining which modes appear. Observation of subharmonic formation in terms of the surface tracings is difficult because the subharmonic mode occurs intermittently throughout the tracing. The development of the subharmonic differs in an important way from the occurrence of the overtone. While the overtone will always be present, according to (18), the subharmonic is expected to appear only after the fundamental has reached some critical amplitude. As a consequence, the subharmonic is not expected to grow until some finite distance downstream and is predicted to be associated with the largest-amplitude fundamental modes. The data are consistent with these predictions. The bicoherence spectra, shown in figure 7(*c*), clearly demonstrate the immediate fundamental/first overtone coherence at short fetch, and then much weaker coherence between the fundamental and the subharmonic appearing at the second probe. By the third probe, the magnitude is somewhat decreased but there is still coherence between the subharmonic and the fundamental. This lowering of coherence may result because the subharmonic, as it grows, behaves more as a free mode.

Figure 8 shows wave data when R_L is decreased still further. Behaviour similar to figure 7 occurs with a small subharmonic appearing by the last probe. The bicoherence spectra again show fundamental–overtone coherence followed by an emerging coherence between $f_1 = 10$ and $f_2 = 5$ Hz and also $f_1 = 5$ and $f_2 = 5$ Hz.

Substantially different behaviour can be observed if the liquid viscosity is increased to 20 cP. Figure 9 shows the evolving wave spectrum for a 20 cP liquid at $R_G = 6300$ and $R_L = 5$. It is seen that the magnitude of the power spectrum changes little with distance but that it broadens with the appearance of new sidebands. In addition, the peak at low frequency exhibits continued growth. The bicoherence spectra shown in figure 9(*c*) demonstrate that the low-frequency peak is correlated with sidebands of the main peak (notice the strong contours at $f_1 = 13.5, f_2 = 1$) and indicate that the low-frequency mode is participating in quadratic interactions similar to those shown above which produce subharmonics and overtones. This provides a way for the main peak to feed energy into low-frequency modes that are otherwise stable. Such energy transfer may have important implications to the formation of long-wavelength disturbances which, given further growth, could evolve into roll waves. In addition, the spectra at all three locations show a strong coherence between the fundamental and the first overtone; energy transfer from the fundamental to the first overtone is again the primary mechanism for stabilization of the wave field.

It is also of interest to examine the speed of some of the disturbances. Wave speeds measured using the two-probe set-up with a separation distance of 1.55 cm, at a location 5 m from the channel inlet, for conditions close to those of figures 3 and 8, are shown in figure 10. Figure 10(*a*) shows that the average speed of the overtone is only slightly higher than the fundamental (~ 34 compared to 33 cm/s). In figure 10(*b*) the speed of the lower peak is slightly less than the fundamental. These data show that mode interactions occur even though the modes are not perfectly resonant.

Figure 11 shows a comparison of the measured wave speed from figure 10(*a*) with the prediction of the two limiting forms of linear stability theory. If the predicted wave speed is obtained by smoothly interpolating between the two theoretical curves, then linear stability theory predicts the wave speed relatively well. More importantly, the degree of dispersion, which is small, is likewise well predicted. Data sets for other conditions show similar qualitative behaviour and quantitative agreement with measurements.

6. Discussion

It is of interest to compare quantitative predictions of (4) with experiments. Using the interpolated linear stability of figure 1, and four modes of (4) chosen as $k = 1.4, 2.8, 4.2, 5.6$ (the fundamental and the first three overtones), numerical integration of (4) using a Runge–Kutta routine gives steady amplitude values of 0.047 cm and 0.016 cm for the fundamental and first overtone. The measured values are 0.023 cm and 0.003 cm as determined by integration of the spectrum of figure 3 over the ranges of the two peaks. While the predictions are certainly not exact the agreement can be viewed as quite good, considering that it represents an *a priori* prediction of the wave amplitude in a cocurrent gas–liquid flow where the gas is turbulent. It is seen from (12) that the amplitude of the first mode depends primarily on the $\frac{1}{2}$ power of the growth rate, the mis-match parameter and nonlinear coefficients. Errors in any of these, because the linear and nonlinear theories are not strictly valid, could contribute to the discrepancy between the measurements and predictions. The

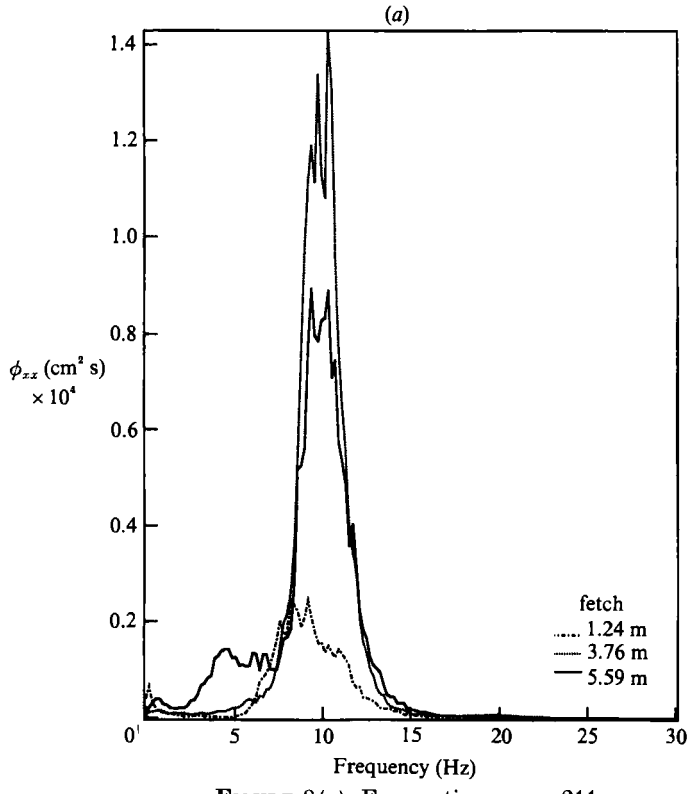

FIGURE 8(*a*). For caption see p. 211.

ability of (4) to accurately describe behaviour is expected to diminish as the liquid layer thickness is decreased. The interaction coefficients definitely cannot be described by (4) because, as showed by Jurman (1990), interaction coefficients for equations derived from boundary-layer equations (valid for $k \to 0$) have both real and imaginary components.

The data in figure 7 show clear evidence of subharmonic instability through the presence of a 5 Hz mode. The bispectral data of figure 7(*c*) suggest that the mechanisms of formation of the subharmonic may involve the $\frac{3}{2}$ mode as well as the fundamental. Note the presence of significant coherence between $f_1 = 10$ Hz and $f_2 = 5$ Hz so that $f_3 = 15$ Hz, the $\frac{3}{2}$ mode. Cheng & Chang (1991) show (their equation (3.23)) that, at least for non-dispersive systems, when the $\frac{1}{2}$, 1 and $\frac{3}{2}$ modes are involved in subharmonic generation, the criterion for instability is still qualitatively similar to (18) with the amplitude of the fundamental again playing a dominant role. Therefore, the observation that the subharmonic mode occurs intermittently in time is consistent with the formation criterion as the amplitude of the fundamental is not constant but varies (apparently) randomly. Larger amplitude fundamental waves are hence more likely to have a subharmonic wave associated with them. This is in contrast with the overtones in figures 5 and 6 which appear with every fundamental. This also explains the higher level of bicoherence between the fundamental and first overtone as opposed to the fundamental and subharmonic. The general question of when to expect subharmonic instability involves several competing factors; the simple observation from the data above, that a subharmonic is more likely to form if the layer thickness is decreased, needs further scrutiny. For the data shown here,

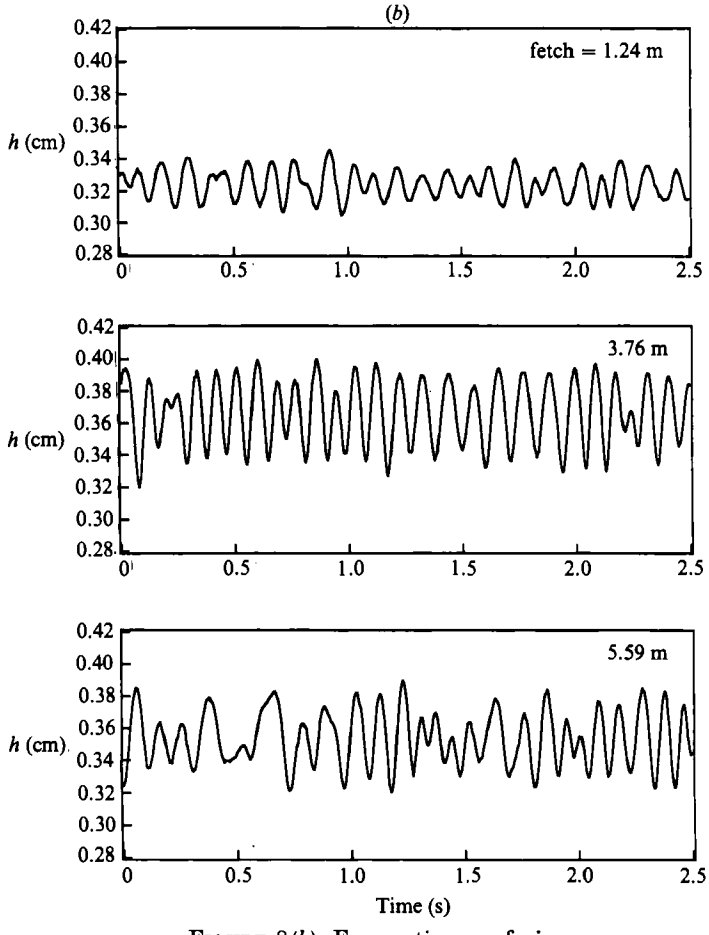

FIGURE 8(b). For caption see facing page.

the amplitude of the fundamental is 0.023 cm in figure 3, 0.034 cm in figure 6, 0.04 cm in figure 7 at the middle probe and 0.025 cm at the middle probe in figure 8. Therefore, both the fundamental mode amplitude and an increase in the value of the interaction coefficient $P_{1,\frac{1}{2}}$, as the layer depth is decreased, explain the formation of the subharmonic.

To demonstrate how the formation of a subharmonic would be predicted by the mode equations from an initially (almost) smooth interface, a calculation for the conditions of figure 7 was done using modes $k = 1.05$ (subharmonic), 2.1 (fundamental), 4.2, 6.3, and 8.4 which have predicted growth rates of -0.05, 1.12, -0.96, -5.603 and $-12.02\ \mathrm{s}^{-1}$ respectively. The initial evolution of the fundamental and subharmonic is shown in figure 12 starting with $a_1 = 0.01$ cm and $a_{\frac{1}{2}} = 0.001$ cm. A logarithmic ordinate is used for clarity at small magnitude. It is seen that, initially, the fundamental grows monotonically until reaching an almost steady value (which would be the steady state in the absence of the $k = 1.05$ mode) while the subharmonic decays. However, once the fundamental has reached a sufficiently large amplitude, the subharmonic begins to grow. The equations then predict oscillations, which may or may not occur in the real system, before a final steady state is reached. One important observation is that a rather abrupt switch in the dominant wavelength can occur, even though the fundamental will persist after the subharmonic grows. A

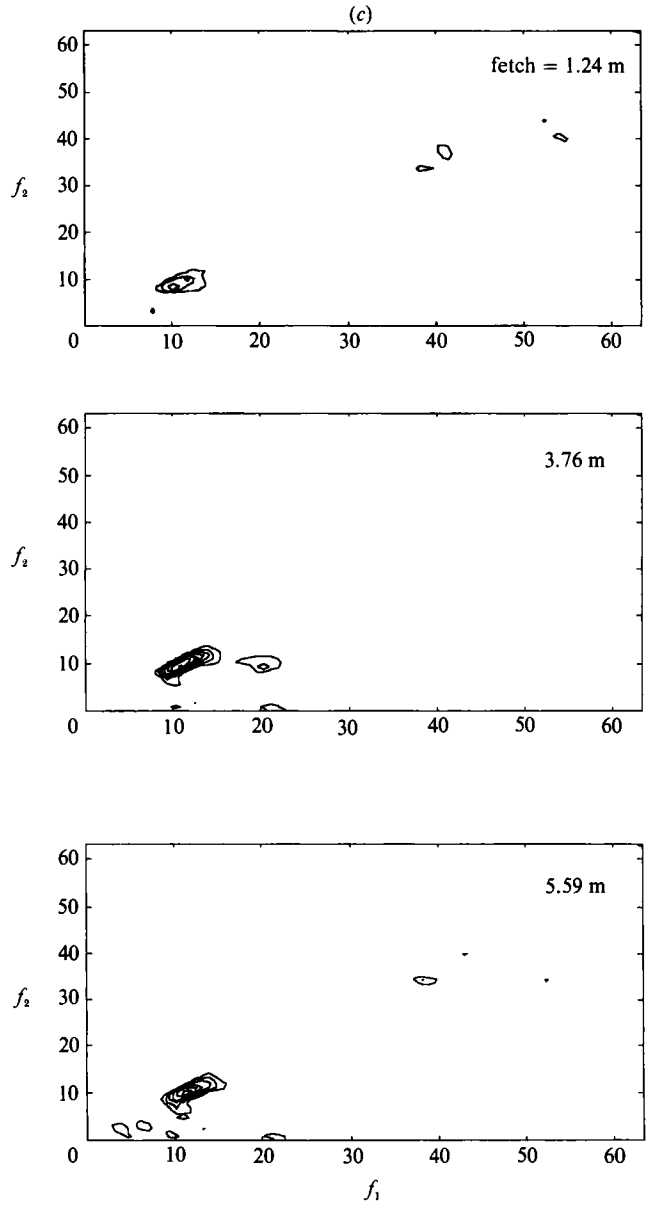

FIGURE 8. (*a*) Wave spectra as a function of fetch. (*b*) Surface tracings as a function of fetch, (*c*) Bicoherence of wave field close to neutral stability (contour lines represent $b^2 = 0.1$). $R_L = 5$, $R_G = 6300$, $h = 0.36$ cm, $U_{air} = 4.3$ m/s, $\mu_L = 10$ cP.

second point is that this transfer occurs even if the fundamental is not in resonance with it subharmonic.

Figure 9 shows evidence of sideband modes which interact with a low-frequency peak that grows with distance. The bispectra demonstrate coherence between the peak sidebands and the low-frequency mode. Because the sidebands appear to be more pronounced at larger distance, it would seem that the spectra are not exhibiting merely a transient state but that the main peak is unstable to sidebands. If the main

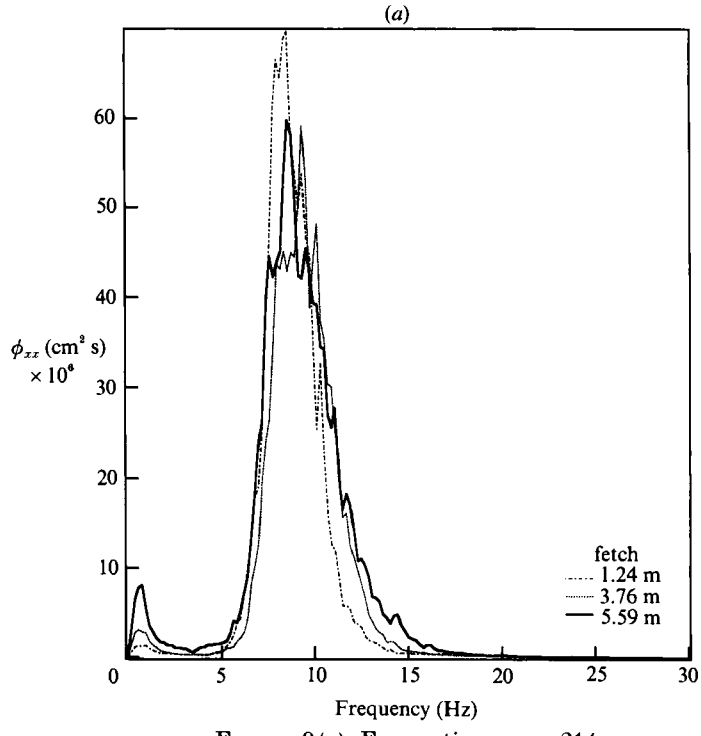

FIGURE 9(*a*). For caption see p. 214.

peak is assumed to be located at the peak in the growth curve, as all of the spectra seem to be, then (19) does not provide any aid in predicting why the main peak is unstable to sidebands, as the main peak is predicted to be stable. However, there are two possible explanations for this apparent discrepancy. Cheng & Chang (1990) mention that the analytical analysis which gives (19) is limited to the region close to neutral stability. It may be that R_G is too large for (19) to be valid. A second possibility is that the δk modes must be included in the initial description of stability. Because (4) are certainly not able to describe modes with such low wavenumbers, this possibility cannot be tested. As was mentioned above, the important implication of these data is that energy is transferred from the main peak to a much longer wavelength disturbance at R_G values substantially below where such waves are predicted to grow from linear stability theory. Under conditions where a low-frequency peak of finite amplitude can receive energy directly from the gas flow, the possibility exists for these waves to grow to significant amplitude – at conditions where they are predicted to be linear stable! While for the thin film of figure 9 this has no adverse implications for flow regime stability, the role of sideband interactions in initiating the formation of slugs, which are often ascribed to linearly unstable long-wavelength waves, deserves further study.

It is possible to speculate about the behaviour of waves on much deeper layers in terms of the theory and experiments presented here. The linear growth rates presented by Gastel *et al.* (1985) are of similar magnitude to those in figure 1. As a consequence, any deviation will result from different magnitudes of L_i, P_i and Q_i. It is not obvious from the form of the equations, but the P_i and Q_i decrease as the depth increases; the L_i are amplified with increasing depth. As a consequence, the steady-state amplitudes will increase as the depth is increased. This will then

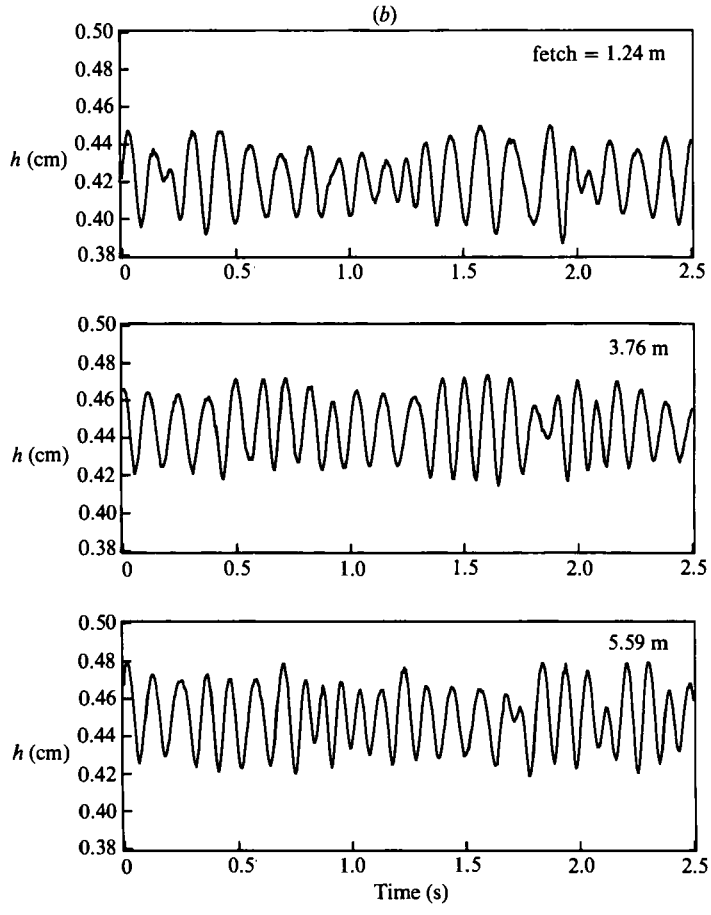

FIGURE 9(*b*). For caption see p. 214.

enhance the possibility that a subharmonic mode will form. It is also noted that, as discussed by Cheng & Chang (1992), more than one subharmonic may form.

The general implication of the data is that all of the interactions shown here, with the addition of the transverse instability, will be important in determining the wave spectrum at conditions far above neutral stability. Therefore, to accurately predict the wave spectrum at arbitrary conditions, theoretical procedures will need to include both linear growth/decay and all of the interactions observed above.

7. Conclusions

Measurements of interfacial waves in cocurrent flows close to neutral stability reveal that the primary mechanism for stabilization of the fastest growing mode is energy transfer to the first overtone which is linearly stable and can dissipate energy. This energy transfer and stabilization occurs even if the two modes are not 'resonant' and can cause the fundamental to stabilize with wave slope as small as ~ 0.005. For other conditions close to neutral stability, a first subharmonic is observed to form and grow with distance. This apparently occurs when energy transfer from interaction between the subharmonic and the fundamental (and perhaps a $\frac{3}{2}$ mode) is strong enough to overcome linear viscous dissipation.

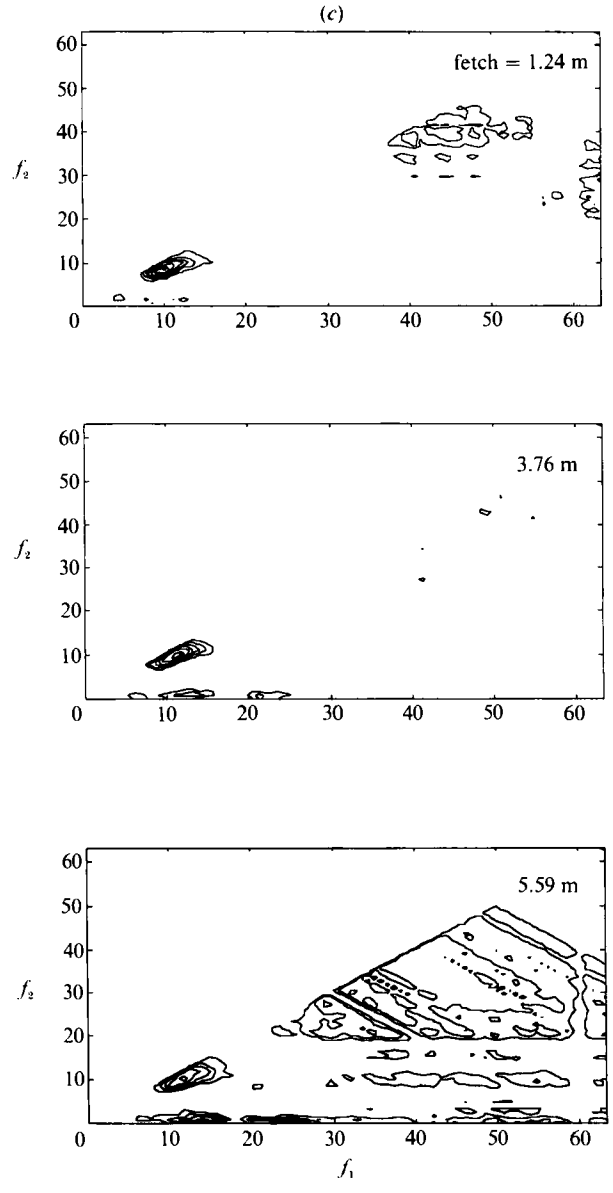

FIGURE 9. (*a*) Wave spectra as a function of fetch. (*b*) Surface tracings as a function of fetch. (*c*) Bicoherence of wave field close to neutral stability; evidence of sideband interactions is seen (contour lines represent $b^2 = 0.1$). $R_L = 5$, $R_G = 6300$, $h = 0.44$ cm, $U_{air} = 4.5$ m/s, $\mu_L = 20$ cP.

Interactions between the sidebands of the fundamental and small-frequency modes may also occur, suggesting that energy can be fed into long-wavelength waves at conditions far below where they are linearly unstable. It is expected that all of these interactions, with the addition of transverse instability, play important roles in determining the behaviour of the spectrum away from neutral stability.

This work is being supported by the Department of Energy under Grant DE FG02-88ER13913. Financial assistance from Chevron Research Company is also acknowledged.

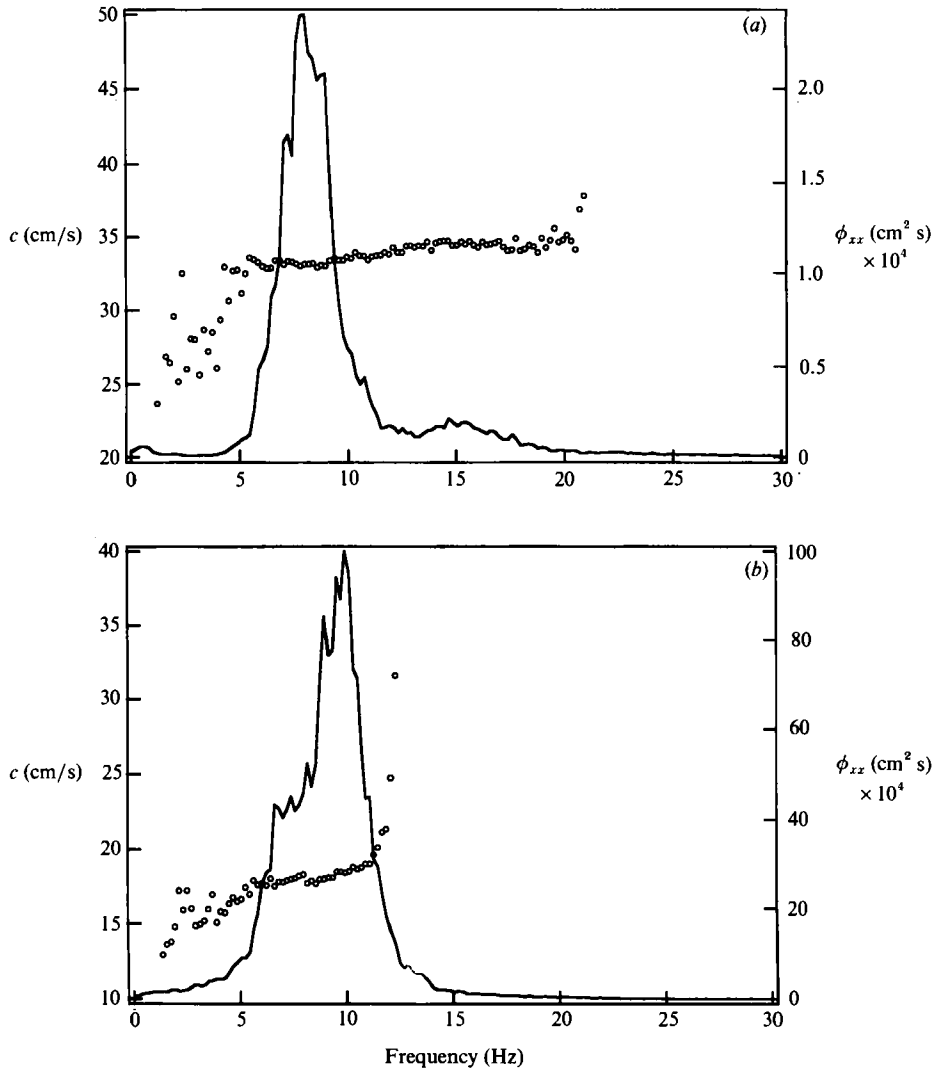

FIGURE 10. Sample dispersion curves (○) with superimposed power spectra (——). (*a*) $R_L = 78$, $R_G = 3640$, $U_{air} = 2.9$ m/s, $h = 0.68$ cm $\mu_L = 10$ cP. (*b*) $R_L = 5$, $R_G = 6300$, $U_{air} = 4.3$ m/s, $h = 0.36$ cm, $\mu_L = 10$ cP.

Appendix

Because the air/liquid density and viscosity ratios are small (they are 0.0012 and 0.0018 for the 10 cP liquid in this study), and in the light of the recently obtained good predictions of the point of neutral stability and wave amplitudes (Prokopiou *et al.* 1992), the behaviour of waves will be described by equations of motion for the liquid phase with the effect of the gas flow entering through boundary conditions.

The pressure and shear stress variations will be taken as sinuous with phase and magnitude obtained from experiments and modelling of turbulent flow over solid wavy surfaces (Thorsness *et al.* 1978; Abrams 1984). The pressure and shear stress variations are denoted as

$$p' = \hat{p}\exp[ik(x-ct)], \quad \hat{p} = \hat{p}_R + i\hat{p}_I, \qquad (A\ 1a, b)$$

$$\tau' = \hat{\tau}\exp[ik(x-ct)], \quad \hat{\tau} = \hat{\tau}_R + i\hat{\tau}_R, \qquad (A\ 1c, d)$$

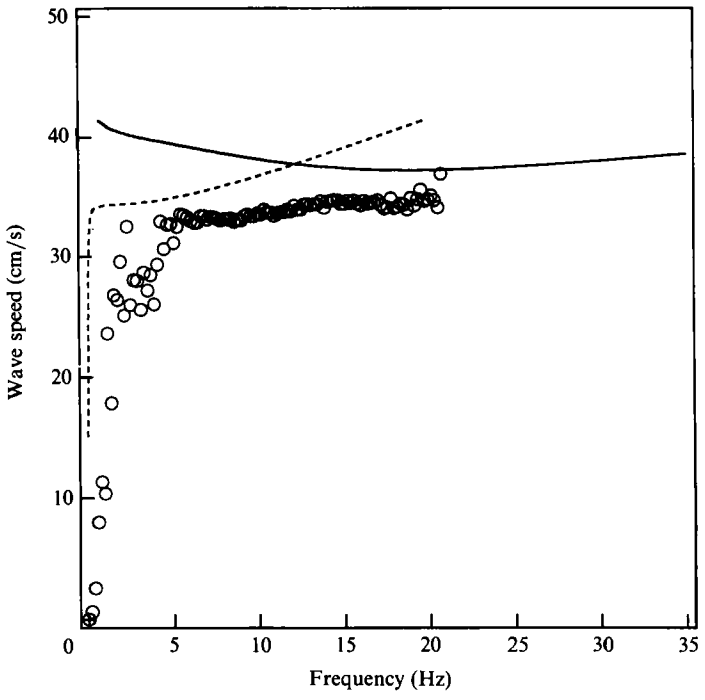

FIGURE 11. Comparison of measured wave speed (○) with prediction of linear stability theory (……, boundary layer; ——, deep layer): $R_L = 78$, $R_G = 3640$, $h = 0.68$ cm, $\mu_L = 10$ cP.

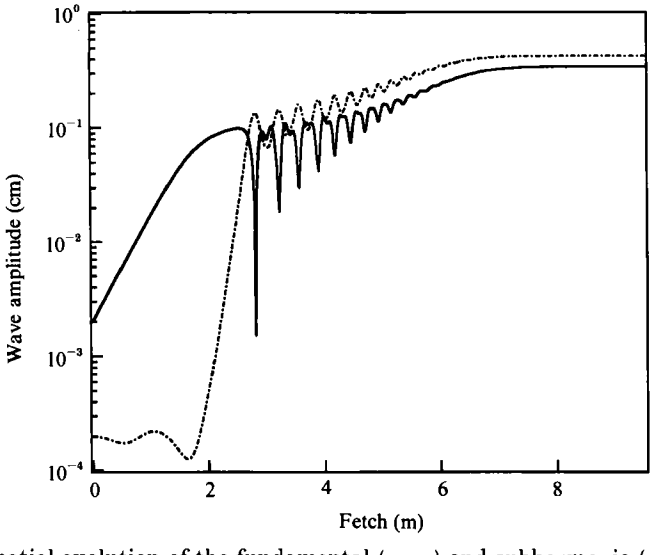

FIGURE 12. Spatial evolution of the fundamental (——) and subharmonic (—·—·—) as predicted by (4) for condition where a subharmonic is observed experimentally. Note that the subharmonic does not begin to grow until the fundamental has reached a threshold amplitude which is in qualitative agreement with (18).

where p' is the wave-induced variation in the dynamic gas phase pressure P, and τ' is the wave-induced variation in the interfacial stress, τ. The boundary condition for interfacial stress can be written as

$$\tau = \frac{1}{R_L}\left(U_0' + \frac{\partial u'}{\partial y} + \frac{\partial v'}{\partial x} + \eta\frac{\partial^2 U_0}{\partial y^2}\right) \quad \text{for} \quad y = \eta, \tag{A 2}$$

where u' and v' are the wave-induced tangential and normal velocity fluctuations and η is the surface position. The pressure boundary condition is

$$P = p - g\eta + T\nabla\cdot\left(\frac{\eta}{(1+(\nabla\eta)^2)^{\frac{1}{2}}}\right) - \frac{1}{R_L}\tau_{yy}, \tag{A 3}$$

where p is the pressure in the liquid phase and τ_{yy} is the normal viscous stress. The kinematic condition at the interface is

$$\left(\frac{\partial}{\partial t} + u'\frac{\partial}{\partial x}\right)\eta = v'. \tag{A 4}$$

The flow of interest is confined to a finite-depth channel. At the bottom wall, the conditions on the liquid velocity are

$$u' = v' = 0 \quad \text{at} \quad y = -h \tag{A 5}$$

A.1. *Linear stability*

For the linear stability problem, all fluctuating variables (e.g. u') will be written as

$$u' = \hat{u}\exp\left[\mathrm{i}k(x - ct)\right], \tag{A 6}$$

where k is real and c is complex. Cohen & Hanratty (1965) provide an analytical solution, for the wave speed $\mathrm{Re}\,[c]$ and growth rate $k\,\mathrm{Im}\,[c]$ for large kR_L if $U_0'' = 0$. These expressions are given in §2.2 as (2) and (3). A more general version of this solution, which contains additional powers of $1/R_L$, is given by Hanratty (1983).

A.2. *Nonlinear evolution*

A set of quadratic evolution equations for the complex mode amplitudes A_1 can be derived following the multiple scale procedure of Janssen (1986) in which time and distance variables are expanded in powers of the wave slope. For the present analysis it is assumed that the pressure and shear variations caused by the gas flow are satisfied exactly at linear order, so that τ' and p' will not enter into the nonlinear problem, and that kR_L is large enough that viscous effects may be neglected at second order in wave slope. For the derivation to be valid, it is necessary that mode growth/damping rates, nonlinear energy transfer and mode speed dispersion all be confined to the same order – which in this case is $1/hkR_L$. Also, because the available linear stability was formulated temporally, the complex mode amplitudes will be functions of t but not x.

The derivation proceeds by expanding the above boundary conditions along with the Navier–Stokes equations. Janssen (1986) provides details of how to accomplish this derivation. The major differences for our case are that the modes are allowed to be dispersive, which leads to the L_l term in (4), and the presence of a bottom wall. A linear velocity profile is assumed from the outset to enable a completely analytical solution. This simplification is expected to cause no qualitative change in (4).

REFERENCES

ABRAMS, J. 1984 Turbulent flow over small amplitude solid waves. Ph.D. thesis, Department of Chemical Engineering, University of Illinois, Urbana.

BANNERJEE, P. P. & KORPEL, A. 1982 Subharmonic generation by resonant three-wave interaction of deep-water capillary waves. *Phys. Fluids* **25**, 1938–1943.

BENDAT, J. S. & PIERSOL, A. G. 1986 *Random Data: Analysis and Measurement Procedure*, 2nd edn. John Wiley.

BENJAMIN, T. B. 1959 Shearing flow over a wavy boundary. *J. Fluid Mech.* **6**, 161–205.

BENJAMIN, T. B. & FEIR, J. E. 1967 The disintegration of wave trains on deep water. Part 1. Theory. *J. Fluid Mech.* **27**, 417–430.

BLENNERHASSETT, P. J. 1980 On the generation of waves by wind. *Proc. R. Soc. Lond.* A **298**, 451–494.

BLENNERHASSETT, P. J. & SMITH, F. T. 1987 Short-scale waves on wind-driven water ('cat's paws'). *Proc. R. Soc. Lond.* A **410**, 1–17.

BONTOZOGLOU, V. & HANRATTY, T. J. 1990 Capillary–gravity Kelvin–Helmholtz waves close to resonance. *J. Fluid Mech.* **217**, 71–91.

BRUNO, K. 1988 The study of interfacial waves in gas-liquid flows. Ph.D. thesis, University of Notre Dame.

BRUNO, K. & MCCREADY, M. J. 1988 Origin of roll waves in gas–liquid flows. *AIChE J.* **34**, 1431–1440.

BRUNO, K. & MCCREADY, M.. J. 1989 Processes which control the interfacial wave spectrum in separated gas-liquid flows. *Intl J. Multiphase Flow* **15**, 531–552.

CHEN, B. & SAFFMAN, P. G. 1979 Steady gravity–capillary waves on deep water – I. Weakly nonlinear waves. *Stud. Appl. Maths* **62**, 95–111.

CHENG, M. & CHANG, H.-C. 1990 A generalized sideband stability theory via center manifold projection. *Phys Fluids* A **2**, 1364–1379.

CHENG, M. & CHANG, H.-C. 1992 Subharmonic instabilities of spatially periodic states. *Phys. Fluids* (to appear).

CHOI, I. 1977 Contributions a l'etude des mechanisms physiques de la generation des ondes de capillarite-gravite a une interface air-eau. Thesis, Université D'Aix Marseille.

COHEN, L. S. & HANRATTY, T. J. 1965 Generation of waves in the concurrent flow of air and a liquid. *AIChE J.* **11**, 138–144.

CRAIK, A. D. D. 1966 Wind-generated waves in thin liquid films. *J. Fluid Mech.* **26**, 369–392.

EKHAUS, W. 1965 *Studies in Nonlinear Stability Theory*. Springer.

ELGAR, S. & GUZA, R. T. 1985 Observations of bispectra of shoaling surface gravity waves. *J. Fluid Mech.* **161**, 425–448.

GASTEL, K. VAN, JANSSEN, P. A. E. M. & KOMEN, G. J. 1985 On phase velocity and growth rate of wind-induced gravity-capillary waves. *J. Fluid Mech.* **161**, 199–216.

GASTEL, K. VAN 1987 Nonlinear interactions of gravity-capillary waves: Lagrangian theory on effects on the spectrum. *J. Fluid Mech.* **182**, 499–523.

GASTER, M. 1962 A note on the relation between temporally-increasing and spatially-increasing disturbances in hydrodynamic stability. *J. Fluid Mech.* **14**, 222–224.

GUCKENHEIMER, J. & HOLMES, P. 1983 *Nonlinear Oscillations, Dynamical Systems, and Bifurcations of Vector Fields*. Springer.

HANRATTY, T. J. 1983 Interfacial instabilities caused by air flow over a thin liquid layer. In: *Waves on Fluid Interfaces* (ed. R. E. Meyer), pp. 221–259. Academic.

HENDERSON, D. M. & HAMMACK, J. L. 1987 Experiments on ripple instabilities. Part 1. Resonant triads *J. Fluid Mech.* **184**, 15–41.

HUERRE, P. 1987 Spatio-temporal instabilities in closed and open flows. In *Instabilities and Nonequilibrium structures* (ed. E. Tirapegui & D. Villarroel), pp. 141–177. Reidel.

HUERRE, P. & MONKEWITZ, P. A. 1985 Absolute and convective instabilities in free shear layers. *J. Fluid Mech.* **159**, 151–168.

HUGHES, D. W. & PROCTOR, M. R. E. 1990 Chaos and the effect of noise in a model of three-wave mode coupling. *Physica* D **46**, 163–176.

JANSSEN, P. A. E. M. 1986 The period-doubling of gravity–capillary waves. *J. Fluid Mech.* **172**, 531–546.

JANSSEN, P. A. E. M. 1987 The initial evolution of gravity–capillary waves. *J. Fluid Mech.* **184**, 581–597.

JURMAN, L. A. 1990 Interfacial waves on sheared, thin liquid films. Ph.D. thesis, University of Notre Dame.

JURMAN, L. A. & MCCREADY, M. J. 1989 Study of waves on thin liquid films sheared by turbulent gas flows. *Phys. Fluids* A **1**, 522–536.

KAWAI, S. 1979 Generation of initial wavelets by instability of a coupled shear flow and their evolution to wind waves. *J. Fluid Mech.* **93**, 661–703.

KIM, Y. Y. & HANRATTY, T. J. 1971 Weak quadratic interactions of two-dimensional waves. *J. Fluid Mech.* **50**, 107–132.

KIM, Y. C. & POWERS, E. J. 1979 Digital bispectral analysis and its applications to nonlinear wave interactions. *IEEE Trans. Plasma Sci.* **PS-7**, 120–131.

LANGE, C. G. & NEWELL, A. C. 1974 A stability criterion for envelope equations. *SIAM J. Appl. Maths* **27**, 441–456.

LIN, S. P. 1974 Finite amplitude side-band stability of a viscous film. *J. Fluid Mech.* **63**, 417–429.

LLEONART, G. T. & BLACKMAN, D. R. 1980 The spectral characteristics of wind-generated capillary waves. *J. Fluid Mech* **97**, 455–479.

MCCREADY, M. J. 1986 Spectral behavior of capillary waves in gas–liquid flows. *Phys. Fluids* **29**, 2836–2842.

MCGOLDRICK, L. F. 1965 Resonant interactions among capillary–gravity waves. *J. Fluid Mech.* **21**, 305–331.

MCGOLDRICK, L. F. 1970 An experiment on second-order capillary gravity resonant wave interactions. *J. Fluid Mech.* **40**, 251–271.

MILES, J. W. 1957 On the generation of surface waves by shear flows. *J. Fluid Mech.* **3**, 185–204.

MIYA, M., WOODMANSEE, D. E. & HANRATTY, T. J. 1971 A model for roll waves in gas–liquid flows. *Chem. Engng Sci.* **26**, 1915–1931.

PHILLIPS, O. M. 1985 Spectral and statistical properties of the equilibrium range in wind-generated gravity waves. *J. Fluid Mech.* **156**, 505–531.

PRESS, W. H., FLANNERY, B. P., TEUKOLSKY, S. A. & VETTERLING, W. T. 1986 *Numerical Recipes: The Art of Scientific Computing*. Cambridge University Press.

PROKOPIOU, TH., MCCREADY, M. J. & CHANG, H.-C. 1992 Wave transitions on horizontal gas sheared liquid films. *J. Fluid Mech.* (submitted).

QIAN, J. 1983 Variational approach to the closure problem of turbulence theory. *Phys. Fluids* **26**, 2098–2108.

SIMMONS, W. F. 1969 A variational method for weak resonant wave interactions. *Proc. R. Soc. Lond.* A **309**, 551–575.

STUART, J. T. & DIPRIMA, R. C. 1978 The Eckhaus and Benjamin–Feir resonance mechanisms. *Proc. R. Soc. Lond.* A **362**, 27–41.

THORSNESS, C. B., MORRISROE, P. E. & HANRATTY, T. J. 1978 A comparison of linear theory with measurements of the variation of shear stress along a solid wave. *Chem. Engng Sci.* **33**, 579–592.

VALENZUELA, G. R. 1976 The growth of gravity–capillary, waves in the coupled shear flow, *J. Fluid Mech.* **76**, 229–250.

VALENZUELA, G. R. & LAING, M. B. 1972 Nonlinear energy transfer in gravity–capillary wave spectra, with applications. *J. Fluid Mech.* **54**, 507–520.

VYSHKIND, S. YA. & RABINOVICH, M. I. 1976 The phase stochastization mechanism and the structure of wave turbulence in dissipative media. *Sov. Phys. JETP* **44**, 292–299.

WERSINGER, J.-M., FINN, J. M. & OTT, E. 1980 Bifurcation and "strange" behaviour in instability saturation by nonlinear three-wave mode coupling. *Phys. Fluids* **23**, 1142–1154.

WIGGINS, S. 1990 *Introduction to Applied Nonlinear Dynamical Systems and Chaos*. Springer.